Crossovers and phase transitions in Bose-Fermi mixtures

by

Boniface Dimitri Christel Kimene Kaya

Thesis presented in partial fulfilment of the requirements for the degree of Master of Science in the Faculty of Science at Stellenbosch University.

Supervisors:

Dr. Alexander V. Avdeenkov
Dr. Johannes N. Kriel

April 2014

Declaration

By submitting this thesis electronically, I declare that the entirety of the work contained therein is my own, original work, that I am the sole author thereof (save to the extent explicitly otherwise stated), that reproduction and publication thereof by Stellenbosch University will not infringe any third party rights and that I have not previously in its entirety or in part submitted it for obtaining any qualification.

Date: January 2014 .....

Abstract

Crossovers and phase transitions in Bose-Fermi mixtures

B.D.C Kimene Kaya

Thesis: MSc

April 2014

We present a theoretical approach that allows for the description of trapped Bose-Fermi mixtures with a tunable interspecies interaction in the vicinity of a Feshbach resonance magnetic field.The many-body physics of the system is treated at equilibrium using the well-established mean-field and local density approximations. This reduces the physics locally to that of a homogeneous system. We observe a rich local phase structure exhibiting both first and second order phase transitions between the normal and BEC phases. We also consider the global properties of the mixture at a fixed number of particles and investigate how the density profiles and the populations of the various particle species depend on the detuning and trap profile.

Uittreksel

Oorkruising en fase-oorgange in gevangde Bose-Fermi mengsels

B.D.C Kimene Kaya

Tesis: MSc

April 2014

Ons beskou 'n teoretiese beskrywing van gevangde Bose-Fermi mengsels met 'n verstelbare interspesie wisselwerking in die teenwoordigheid van 'n magneties-geïnduseerde Feshbach resonansie. Die veeldeeltjiefisika van die sisteem word by ekwilibrium binne die welbekende gemiddelde-veld en lokale-digtheid benaderings hanteer. Sodoende word die fisika lokaal tot die van 'n homogene sisteem gereduseer. Ons neem 'n ryk fase-struktuur waar met beide eerste- en tweede-orde fase-oorgange tussen die normale en BEK fases. Ons beskou ook die globale eienskappe van die mengsel by 'n vaste totale aantal deeltjies en ondersoek hoe die digtheidsprofiele en deeltjiegetalle van die afstemming en die profiel van die val afhang.

Acknowledgements

All praise is for **God**, the Exalted, without whom the completion of this project would have not been possible.
I am also greatly indebted to my supervisor Dr. A. A. Alexander for suggesting this exciting essay topic.

I would like to express my sincere thanks to my co-supervisor Dr J.N. Kriel for his simplicity and encouragement to motivate me through out my MSc project. He has shown me his tremendous guidance, patience and numerous open discussions, which contributed to the success of my work. He has taught me most of what I know in Mathematica during my simulations, and also for his kindness with many of my insignificant questions.
I would like also to thank all the department members and colleagues for the time they spent to help me.

I feel so privileged for having received funding from the Department of Physics through the National Institute of Physics (NITheP) and Stellenbosch University. This helped me to immerse myself in research.
Finally I would like to thank my family, and specially Mr Cyrille Kimposso and Mr Boniface Kaya for their encouragements and support. My son Nathan Kimene whom I missed for many years away from home.

Contents

List of Figures

List of Tables

Chapter 1

Introduction

Since the realization of Bose-Einstein condensation in trapped atomic gases of the same species in past years [1, 2], the trapping and cooling have been extended for mixtures of bosons and fermions. This has opened new directions in the field of ultracold gases. The mixtures have stimulated the study of quantum phenomena such as many-body physics and are not fully understood. Such systems behave differently from boson-boson to fermion-fermion gases of the same species. One of the characteristic of these mixtures is, for two species with different magnetic moments, the interaction between particles is tuned by varying the magnetic field with the use of Fano-Feshbach resonances [3, 4, 5, 6]. In this regime of tunable interactions, there is an interesting competition between boson-fermion pairing correlations and boson-boson pairing correlations happening in the mixtures. These resonances enable the creation of molecular dimers.

Theoretically the mixtures of bosons and fermions were restricted to dilute non resonant effects of trapped system [7, 8, 9] where it was shown that the density profiles and the stability of the system is governed by the boson-boson and the boson-fermion s-wave interactions. The interplay between boson-boson and boson-fermion interactions have revealed a rich and complex phase diagram. The mean-field stability for the Bose-Fermi mixtures at finite temperatures was investigated. For the dilute binary trapped mixtures, the equilibrium properties have been analysed through the Hartree-Fock-Bogoliubov within the Popov approximation. The finite temperatures greatly affect the critical density and the critical attractive boson-fermion scattering length as demonstrated in Refs. [10, 11]. The formation of the stationary boson-fermion condensate is studied at zero temperature and the appearance of the bright fermionic solitons is made possible when the boson-fermion interactions become attractive[12, 13]. The quantized vortices in the bosonic densities and the maximum reached in the fermionic density, which characterized the Landau-level-regime were studied, including the static properties of a homogeneous boson-fermion attractive interacting gases, have been studied by using the green function formalism [14, 15].
In Refs. [16, 17, 18, 19, 20, 21], it was demonstrated that the exchange of the boson density fluctuations gives rise to an attractive boson-fermion interaction, which causes the transition temperature to increase. For the spin-polarized fermions in the Bose-Fermi mixtures, the temperature of the p-wave Cooper pairing have been achieved and agree with experiments. The superconduct-

ing phase and the Cooper instability in the s-wave have been analysed. The mixtures have shown a rich phase transitions in optical lattices [22, 23]. Indeed, the mean-field criterion and the linear stability of a bosonic superfluid transition were studied [24, 25]. We have seen in Ref. [26] when the fermionic species exceed, the phase coherence of the bosonic atoms diminishes and the density of bosons in the lattice increases for the attractive boson-fermion interactions. One can also identify various quantum phases which depend on the strength of the boson-boson and the boson-fermion repulsive interactions [27, 28].

The mean-field approach in the case of resonant boson-boson [29, 30] and fermion-fermion [31, 32, 33, 34, 35, 36] gases have been thoroughly studied where Feshbach molecules are bosons in both cases. The assumptions are made such that bosonic molecules are fully condensed.
However, with Bose-Fermi mixtures, several approaches have been proposed already with broad resonances in which the Feshbach resonance coupling goes to infinity as analysed in Refs. [37, 38, 39, 40].
For narrow resonances, the mean-field resonant case was already investigated by studying the equilibrium properties and the dynamics of the system in homogeneous cases at zero temperature by using the so-called Harthree-Fock-Bogoliubov formalism [41, 42], including the pairing and condensation [37]. Experiments with Fano-Feshbach resonances have been widely performed for trapped systems of mixtures [43, 44]. From the theoretical point of view, mixtures exhibit a variety of phase transitions that depend on the densities of species and the total number of individual species.

Here we will mainly focus on phase transitions with narrow resonances in which atoms experience different scattering lengths for finite width of resonances. The mixtures here are made out of single-component of bosons and fermions confined in the external potential. We will see that the pairing between the two different species is made favourable by tuning the interaction around Feshbach resonances. We analyse density profiles of various species and study the population evolution as the function of the detuning.

The thesis is structured in the following way:

Chapter 2: Basics of scattering theory.
In this chapter we will give an overview on scattering theory in neutral alkali atoms. The resonant case, specially in the low-energy limit characterized by one parameter called the *scattering length* relevant for ultra cold gases, will be discussed. A simple theoretical treatment to Fano-Feshbach resonances modelled by two spherical attractive potentials well will be given. It is of the great interest because many scenarios are observed when manipulating interactions between atoms in different hyperfine states.

Chapter 3: Trapped Bose-Fermi mixtures in the vicinity of Feshbach resonances.
This chapter is the main body of this thesis. We analyse the mixtures trapped in an anisotropic harmonic potential at zero temperature, through mean-field theory and the local density approximation. We search for possibility of phase transitions, the density profiles of various species. We disregard the region beyond the mean-field approach where three-body correlations have to be

taken into account properly. The case of vanishing coupling that corresponds to the unitary limit will also be disregarded. We will focus mainly on the non vanishing coupling for weakly interacting Bose-Fermi systems. For trapped atomic systems, the momentum is no longer a good quantum number due to the trapping potential that breaks down the symmetry of the system. We will use the local density approximation which makes the system locally homogeneous. Finally, we study the global proprieties of the entire system for different values of the detuning and for a given value of the trap aspect ratio of the oscillator. This asymmetry parameter (trap aspect ratio) is defined as the ratio of the transverse and axial frequencies of the anisotropic trap.

Chapter 4: Conclusions and outlook.
This chapter summarizes the results obtained throughout the thesis, including all relating limitations of the mean field treatment, and also some possible future directions.

Chapter 2

Basics of scattering theory

The elastic scattering of atoms which interact via an inter-atomic potential form the basis of understanding the kinetic properties of dilute quantum gases. In the limit of low densities, only binary interactions are relevant and atoms interact pairwise. Hence the condition of diluteness, which means the range r_0 of the interacting potential is much smaller than the inter-particle distance, is satisfied and the gas is ideal or weakly interacting. Indeed the probability of finding three particles simultaneously in the range r_0 can be neglected.

The aim of this chapter is to investigate the collisional properties of atoms. At first sight the collisional process of two atoms depends not only on the inter-atomic potential but also on the internal properties of the particles as well as their statistics. For ultra cold gases in their electronic ground states only hyperfine structures are adequate and we discuss the resonance in the single channel case. We consider only atoms that are in the same internal state and we will show the divergent behaviour of the scattering length. The scattering of atoms with different internal states, i.e. multichannel problem, will give rise to Feshbach resonances. This will be discussed in detail, since it is of great interest for a system of mixtures of bosons and fermions. We will show in detail that, at low energy, the scattering properties depend only on one parameter: the *scattering length*.

2.1 Scattering of two distinguishable atoms

Consider the scattering of two different spinless atoms, for example the case of two different isotopes of the same atomic species. Since atoms are different, the pair wave function does not need to be symmetric or antisymmetrc.

Our starting point is the time-independent Schrödinger equation written as

$$\left[\hat{H}_0 + \hat{V}\right] |\psi\rangle = E|\psi\rangle \tag{2.1.1}$$

where $\hat{H}_0 = \hat{p}^2/2\mu$ stands for the relative kinetic energy operator of the two colliding atoms. In the absence of the scattering potential ($V = 0$), the solution of the above Schrödinger equation is

just a free particle plane wave state $|\mathbf{k}\rangle$ associated with energy $E = \hbar^2 k^2/2\mu$.

For a non vanishing scattering potential, the formal solution, is

$$|\psi^{(+)}\rangle = |\mathbf{k}\rangle + V\frac{1}{E - \hat{H}_0 + i\varepsilon}|\psi^{(+)}\rangle \tag{2.1.2}$$

known as the $Lippmann - Schwinger$ equation.

The energy in the denominator is made slightly complex and positive to ensure that the scattered wave has only the outgoing terms. Hence we can see that, for $V \longrightarrow 0$, we have $|\psi^{+}\rangle \longrightarrow |\mathbf{k}\rangle$, which is the solution to the free particle Schrödinger equation. More details and the following steps can be found in Ref. [45, 46, 47].

We restrict ourselves to the relative position basis by multiplying from the left of each member of Eq.(2.1.2) by $\langle\mathbf{r}|$ to obtain

$$\langle\mathbf{r}|\psi^{(+)}\rangle = \langle\mathbf{r}|\mathbf{k}\rangle + \frac{2\mu}{\hbar^2}\int \mathbf{d^3}\mathbf{r}' G(\mathbf{r},\mathbf{r}')\langle\mathbf{r}'|V|\psi^{(+)}\rangle, \tag{2.1.3}$$

where

$$G(\mathbf{r},\mathbf{r}') = \frac{\hbar^2}{2\mu}\left\langle \mathbf{r}\left|\frac{1}{E - \hat{H}_0 + i\varepsilon}\right|\mathbf{r}'\right\rangle \tag{2.1.4}$$

is the kernel of the equation defined above. Following the arguments in Ref. [45], for a finite range potential that depends only on the relative position of the atoms, we finally obtain, at large separation ($r \longrightarrow \infty$),

$$\langle\mathbf{r}|\psi^{(+)}\rangle \sim \langle\mathbf{r}|\mathbf{k}\rangle - \frac{1}{4\pi}\frac{2\mu}{\hbar^2}\frac{e^{ikr}}{r}\int \mathbf{d^3}\mathbf{r}' e^{-i\mathbf{k}'\cdot\mathbf{r}'}V(\mathbf{r}')\langle\mathbf{r}'|\psi^{(+)}\rangle. \tag{2.1.5}$$

If we work in the fixed centre-of-mass frame as done by Ref. [48], shown in Fig.2.1, clearly, the wave function for the steady-state, at large distances given above contains both the incident plane-wave

$$\psi_{int}(\mathbf{r}) = \langle\mathbf{r}|\mathbf{k}\rangle \equiv e^{i\mathbf{k}\cdot\mathbf{r}} \tag{2.1.6}$$

with relative kinetic energy and relative momentum given by

$$E = \frac{\hbar^2 k^2}{2\mu} \tag{2.1.7}$$

and

$$\mathbf{p} = \hbar\mathbf{k}, \tag{2.1.8}$$

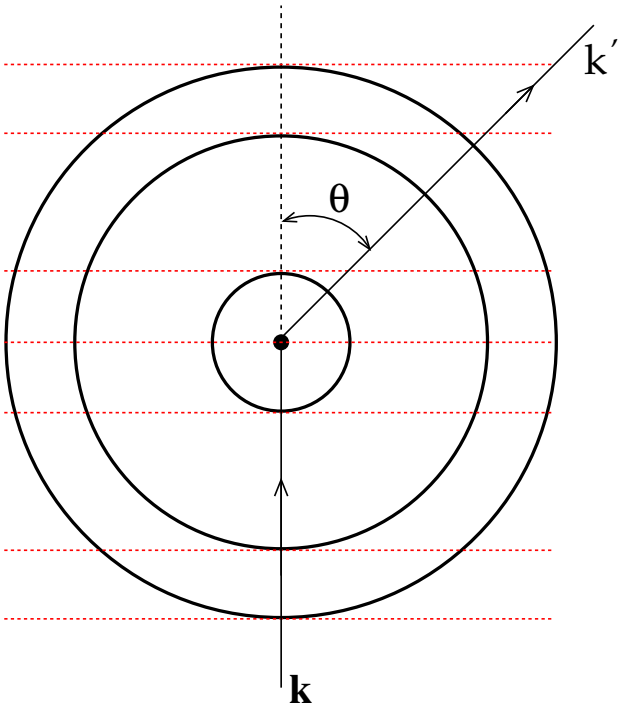

Figure 2.1: *Sketch of collision in the center-of-mass frame. The two atoms enter the scattering center surrounded by the black circle with relative momentum* $\mathbf{k}$*, and scatter as an outgoing spherical wave with relative momentum* $\mathbf{k}'$*. The angle between* $\mathbf{k}$ *and* $\mathbf{k}'$ *is* θ

where μ is the reduce mass, and the *outgoing* anisotropic scattered wave,

$$\psi_{sc}(\mathbf{r}) \sim f(\mathbf{k}', \mathbf{k}) \frac{e^{ikr}}{r}. \tag{2.1.9}$$

The modulation factor $f(\mathbf{k}', \mathbf{k})$, defined by

$$f(\mathbf{k}', \mathbf{k}) \equiv -\frac{1}{4\pi} \frac{2\mu}{\hbar^2} \int d^3\mathbf{r}' e^{-i\mathbf{k}'\cdot\mathbf{r}'} V(\mathbf{r}') \langle \mathbf{r}' | \psi^{(+)} \rangle = -\frac{1}{4\pi} \frac{2m}{\hbar^2} \langle \mathbf{k}' | V | \psi^{(+)} \rangle, \tag{2.1.10}$$

represents the scattering amplitude and depends on the angle θ between $\mathbf{k}$ and $\mathbf{k}' \equiv k'\hat{r}$. It will later be used to determine the scattering cross section.

The magnitude of the wave number $|\mathbf{k}| = k$ has to be conserved because of the energy conservation, and primarily we consider the elastic scattering for dilute gases.

The asymptotic form of the wave function $\psi(\mathbf{r}) \equiv \langle \mathbf{r} | \psi \rangle$ that contains both the incoming plane wave in Eq.(2.1.6) and the outgoing scattered wave in Eq.(2.1.9) can be written as

$$\psi(\mathbf{r}) \sim \psi_{in}(\mathbf{r}) + \psi_{sc}(\mathbf{r}). \tag{2.1.11}$$

The wave function expressed in Eq.(2.1.11) has the asymptotic behaviour at large separation $(r \to \infty)$ given by:

$$\psi(\mathbf{r}) \sim e^{i\mathbf{k}\cdot\mathbf{r}} + f(\mathbf{k}', \mathbf{k}) \frac{e^{ikr}}{r}. \tag{2.1.12}$$

When V is sufficiently weak, then $\langle \mathbf{r}'|\psi^+\rangle$ will be slightly perturbed away from the incident plane wave $\langle \mathbf{r}'|\mathbf{k}\rangle = e^{i\mathbf{k}\cdot\mathbf{r}'}$. After substitution into Eq.(2.1.10), it will yield the well known **first-order Born amplitude** of the form

$$f^{(1)}(\mathbf{k}',\mathbf{k}) = -\frac{1}{4\pi}\frac{2\mu}{\hbar^2}\int d^3\mathbf{r}' e^{i(\mathbf{k}-\mathbf{k}')\cdot\mathbf{r}'}V(\mathbf{r}') = -\frac{1}{4\pi}\frac{2\mu}{\hbar^2}\langle \mathbf{k}'|V|\mathbf{k}\rangle. \tag{2.1.13}$$

$f^{(1)}$ is just the three-dimensional Fourier transform of the potential V apart from the pre-factor in front.

2.1.1 Partial wave expansion

We start with the Schrödinger equation which describes the state of relative motion of the two colliding atoms, written as

$$\left[-\frac{\hbar^2\bigtriangledown^2}{2\mu} + V(\mathbf{r})\right]\psi(\mathbf{r}) = E\psi(\mathbf{r}). \tag{2.1.14}$$

We assume that the interaction potential is spherically symmetric. The wave function solution of the equation above can be factorized into radial and angular parts, depending on r and the angles θ, φ. It has the product form

$$\psi_E(\mathbf{r}) = \sum_{l=0}^{\infty}\sum_{m=-l}^{+l} c_{lm}R_{El}(r)Y_m^l(\theta,\varphi) \tag{2.1.15}$$

called the partial-wave expansion. The coefficient c_{lm} is the normalization constant and R_{El} is the radial function that need to be determined.

The $Y_m^l\ (\theta,\varphi)$ are spherical harmonic functions, which are eigenfunctions of $\hat{L}^2$ and $\hat{L}_z$ explicitly written as

$$Y_m^l(\theta,\varphi) = \frac{(-1)^l}{2^l l!}\sqrt{\frac{2l+1}{4\pi}\frac{(l+m)!}{(l-m)!}}e^{(im\varphi)}\frac{1}{\sin^m\theta}\frac{d^{l-m}}{d(\cos\theta)^{l-m}}(\sin\theta)^{2l}. \tag{2.1.16}$$

We are concerned about wave functions that are in particular axially symmetric along a chosen direction, for example the z-axis, meaning independent of φ. The only terms that can contribute in the sum on the right hand side of Eq.(2.1.15) are those with m=0, and those that are θ dependent, because the potential has a central symmetry. In this case we can write the well known result

$$Y_0^l(\theta) = \frac{1}{2^l l!}\sqrt{\frac{2l+1}{4\pi}}\frac{d^l}{d(\cos\theta)^l}(\cos^2\theta-1)^l = \sqrt{\frac{2l+1}{4\pi}}P_l(\cos\theta), \tag{2.1.17}$$

so that Eq.(2.1.15) becomes

$$\psi(r,\theta) = \sum_{l=0}^{\infty} A_l R_{El}(r) P_l(\cos\theta), \tag{2.1.18}$$

with

$$A_l = \sqrt{\frac{2l+1}{4\pi}} c_l, \tag{2.1.19}$$

where $P_l(\cos\theta)$ are Legendre polynomials and $R_{El}(r)$ are radial wave functions, solutions of the radial Schrödinger equation

$$R''_{El}(r) + \frac{2}{r} R'_{El}(r) + \left[\frac{2\mu E}{\hbar^2} - \frac{l(l+1)}{r^2} - \frac{2\mu}{\hbar^2} V(r)\right] R_{El}(r) = 0. \tag{2.1.20}$$

In particular, if the potential $V(r)$ is vanishing, the radial equation becomes the real Bessel differential equation for $r > r_0$ of the form

$$R''_l(\varrho) + \frac{2}{\varrho} R'_l(\varrho) + \left[1 - \frac{l(l+1)}{\varrho^2}\right] R_l(\varrho) = 0. \tag{2.1.21}$$

Here $\varrho = kr$ is a dimensionless parameter and $k = \sqrt{\hbar^2 E/2\mu}$ is the free particle wave number. Hence, for a short range potential ($V(r) = 0$, for $r > r_0$), the real radial function $R(\varrho)$ for this ordinary linear equation is the combination of two linear independent solutions, the spherical Bessel functions $j_l(\varrho)$ and the spherical Von Neumann functions $n_l(\varrho)$:

$$R_l(kr) = A j_l(kr) + B n_l(kr). \tag{2.1.22}$$

We introduce a dimensionless number $\delta_l = \arctan B/A$ that will have a significant meaning later so that $A = C\cos\delta_l$ and $B = -C\sin\delta_l$. After substitution into Eq.(2.1.22), it yields

$$R_l(kr) = C(\cos\delta_l j_l(kr) - \sin\delta_l n_l(kr)). \tag{2.1.23}$$

The asymptotic forms of the Bessel and Von Neumann functions at large distances are

$$j_l(kr) \sim \frac{\sin(kr - \frac{1}{2}\pi l)}{kr} \tag{2.1.24}$$

and

$$n_l(kr) \sim -\frac{\cos(kr - \frac{1}{2}\pi l)}{kr}, \tag{2.1.25}$$

and therefore, we apply the angle-addition formula for the sine function which leads to the corresponding radial function

$$R_l(kr) \sim \frac{\sin(kr - \frac{1}{2}\pi l + \delta_l)}{kr}. \tag{2.1.26}$$

It is clear that for the vanishing potential, the radial function R_l defined in Eq.(2.1.23) would be valid all the way to $r = 0$, because the function $j_l(kr)$ is regular and well behaved throughout space (including the origin). But the functions $n_l(kr)$ present a singularity at $r = 0$. This is not allowed in a state function, so for all r we require $\delta_l = 0$ if $V(r) = 0$. If we compare the asymptotic form of the zero scattering ($V = 0$) solution, $j_l(kr)$, with the corresponding solution given in Eq.(2.1.26), we note that the main effect of the short range scattering potential is the *phase shift* of the radial function δ_l at large distances .

We now expand the incoming plane wave in terms of Legendre polynomials as described in Ref. [45]. In the expansion of Eq.(2.1.18) we set $R_l(kr) = j_l(kr)$ which is the non-singular solution of the radial spherical Bessel equation. We have

$$\psi(r,\theta) = \sum_{l=0}^{\infty} A_l j_l(kr) P_l(\cos\theta). \tag{2.1.27}$$

The well known result of the plane wave in powers of $kr\cos\theta$ is

$$e^{i\mathbf{k}\cdot\mathbf{r}} = \sum_{l=0}^{\infty} i^l (2l+1) j_l(kr) P_l(\cos\theta). \tag{2.1.28}$$

We then substitute the Bessel functions with their asymptotic forms given in Eq.(2.1.24) and Eq.(2.1.26) into Eq.(2.1.28) and Eq.(2.1.18), giving

$$\psi(r,\theta) = \sum_{l=0}^{\infty} A_l \frac{\sin(kr - \frac{1}{2}\pi l + \delta_l)}{kr} P_l(\cos\theta), \tag{2.1.29}$$

and

$$e^{i\mathbf{k}\cdot\mathbf{r}} = \sum_{l=0}^{\infty} (2l+1) i^l \frac{\sin(kr - \frac{1}{2}\pi l)}{kr} P_l(\cos\theta) \tag{2.1.30}$$

In order to perform our calculations, we must match the asymptotic form of the general solution in Eq.(2.1.18) to Eq.(2.1.12) including the asymptotic forms of the Bessel functions

$$\sum_{l=0}^{\infty} A_l \frac{\sin(kr - \frac{1}{2}\pi l + \delta_l)}{kr} P_l(\cos\theta) = \sum_{l=0}^{\infty} (2l+1) i^l \frac{\sin(kr - \frac{1}{2}\pi l)}{kr} P_l(\cos\theta) + f(\mathbf{k}', \mathbf{k}) \frac{e^{ikr}}{r}. \tag{2.1.31}$$

After expressing the sine functions in terms of complex exponentials using $\sin(x) = (e^{ix} - e^{-ix})/2i$, it yields

$$\begin{aligned} &\sum_{l=0}^{\infty} A_l P_l(\cos\theta) \frac{\exp[i(kr - \frac{1}{2}\pi l + \delta_l)] - \exp[-i(kr - \frac{1}{2}\pi l + \delta_l)]}{2ikr} \\ &\qquad = \sum_{l=0}^{\infty} (2l+1) i^l P_l(\cos\theta) \frac{\exp[i(kr - \frac{1}{2}\pi l)] - \exp[-i(kr - \frac{1}{2}\pi l)]}{2ikr} + f(\mathbf{k}', \mathbf{k}) \frac{e^{ikr}}{r} \end{aligned} \tag{2.1.32}$$

We equate the coefficients of $\exp(-ikr)$ and $\exp(ikr)$ in the equality above, Eq. (2.1.32), term by term. Since the Legendre polynomials are linearly independent, we have

$$A_l = i^l(2l+1)\sin\delta_l \exp(i\delta_l), \tag{2.1.33}$$

$$f(\mathbf{k}', \mathbf{k}) = \sum_{l=0}^{\infty} f_l(k) P_l(\cos\theta), \tag{2.1.34}$$

where the l^{th} component of the partial wave amplitude $f_l(k)$ has the form

$$f_l(k) = \frac{1}{2ik}(2l+1)(e^{2i\delta_l} - 1). \tag{2.1.35}$$

2.1.2 Differential cross section

The quantity in scattering theory that is accessible with current experiments is the scattering cross section. First of all we define the differential cross section as the ratio of the current probability per unit solid angle of particles scattered to the current probability per unit area of incident particles. We have

$$\frac{d\sigma}{d\Omega} d\Omega = \frac{|\mathbf{j}_{sc}|}{|\mathbf{j}_{in}|} r^2 d\Omega, \tag{2.1.36}$$

where the current probability flux is given by

$$\mathbf{j} = \frac{\hbar}{\mu} Im(\psi^* \nabla \psi) \tag{2.1.37}$$

and so, for the incident wave, the uniform probability flux is given by

$$\mathbf{j}_{in} = \frac{\hbar}{\mu} Im\left(\psi_{in}^* \frac{\partial}{\partial r}\psi_{in}\right) = \frac{\hbar}{\mu}\mathbf{k}, \tag{2.1.38}$$

and for the scattered wave, the radial component of the flux is

$$\mathbf{j}_{sc} = \frac{\hbar}{\mu} Im\left(\psi_{sc}^* \frac{\partial}{\partial r}\psi_{sc}\right) = \frac{\hbar k}{\mu}\frac{|f(\mathbf{k}', \mathbf{k})|^2}{r^2}\hat{\mathbf{r}}. \tag{2.1.39}$$

The substitution of the terms obtained from the above fluxes into Eq.(2.1.36) yields the differential cross section

$$\frac{d\sigma}{d\Omega} = |f(\mathbf{k}', \mathbf{k})|^2. \tag{2.1.40}$$

Thus, the total elastic cross section is found after integration of σ over all directions, that is

$$d\Omega = d\phi \sin\theta d\theta \tag{2.1.41}$$

to obtain

$$\sigma = \int_0^{2\pi} d\phi \int_0^{\pi} \sin\theta d\theta |f(\mathbf{k}', \mathbf{k})|^2. \tag{2.1.42}$$

We insert Eq.(2.1.34) into Eq.(2.1.42) and make use of the orthogonality of the Legendre polynomials to obtain

$$\int_0^{\pi} d\theta \sin\theta P_l(\cos\theta) P_{l'}(\cos\theta) = \frac{2}{2l+1}\delta_{ll'}. \tag{2.1.43}$$

The resulting cross section is

$$\sigma(k) = \sum_{l=0}^{\infty} \sigma_l(k) \tag{2.1.44}$$

with

$$\sigma_l(k) = 4\pi(2l+1)|f_l(k)|^2 = \frac{4\pi}{k^2}(2l+1)\sin^2(\delta_l). \tag{2.1.45}$$

Note the connection between the scattering amplitude and the phase shift defined in the cross section of Eq.(2.1.45)

2.1.3 Indistinguishable atoms in the same internal state

Consider the scattering for two identical atomic species in the same internal state. Contrary to the case of atoms of different species, the wave function needs to be either symmetric if the two colliding atoms are bosons or antisymmetric if they are fermions.

In this case, the asymptotic behaviour of the scattering wave function at large distances has the form

$$\psi(\mathbf{r}) \sim e^{i\mathbf{k}\cdot\mathbf{r}} \pm e^{-i\mathbf{k}\cdot\mathbf{r}} + f_{\pm}(\mathbf{k}', \mathbf{k})\frac{e^{ik'r}}{r}. \tag{2.1.46}$$

Where the (+/-) sign refers to bosons(fermions).

The total cross section after expansion in terms of the Legendre polynomials is given by

$$\sigma(k) = \frac{8\pi}{k^2} \sum_{l=even/odd}^{\infty} (2l+1)\sin^2(\delta_l), \tag{2.1.47}$$

where l is *even* for bosons and *odd* for fermions.

Here we have given a general description of the scattering process, but in the following we will be discussing the specific case of low-energy limit and specially the resonant behaviour of the scattering length.

2.2 Resonance scattering in the low-energy limit

2.2.1 Single channel problem

Basically, quantum features of the scattering are dramatically affected by the temperature. The effective interaction in the radial Schrödinger equation, Eq.(2.1.20), contains two terms: The first, $V(r)$, represents the short range interaction between the atom pair that give rise to the phase shift as we have discussed before. The second, $V_{rot} = \hbar^2 l(l+1)/2\mu r^2$, is the centrifugal barrier resulting from the relative angular momentum between the atoms. For ultra-cold alkali atoms, the low energy-limit does not allow them to cross the given centrifugal barrier of the effective potential. In this case only the $l = 0$ (s-wave scattering) contribution to the cross section should be considered. Consequently the scattering amplitude reduces to a constant, $-a$, called the *scattering length* which characterizes the low-energy collision. In this way, the first order in the interaction given in Eq.(2.1.13) will become

$$f(0,0) = -a = -\frac{\mu}{2\pi\hbar^2}\int drV(r), \tag{2.2.1}$$

called the *Born approximation*.
In reality the interatomic potential between two atoms in low-energy limit is very difficult to find because of its complicated dependence on the interparticle distance. Therefore, for two particles located in space at points r and r' the interaction potential can be replaced by the contact $effective\ interaction$ of the form

$$V_{\text{eff}}(\mathbf{r},\mathbf{r}') = U_0\delta(\mathbf{r}-\mathbf{r}'). \tag{2.2.2}$$

We recover the property of low-energy scattering by replacing the potential in the Born approximation, Eq.(2.2.1), with the effective interaction, V_{eff}, thus

$$\int d\mathbf{r}V_{\text{eff}}(\mathbf{r},\mathbf{r}') = \frac{2\pi\hbar^2 a}{\mu} \equiv U_0. \tag{2.2.3}$$

We obtain the well known expression for the s-wave scattering length, resulting from the contact interaction V_{eff} defined as

$$U_0 = \frac{2\pi\hbar^2 a}{\mu}. \tag{2.2.4}$$

Subsequently, Eq. (2.1.12) at large separation, and Eq.(2.1.35) become

$$\lim_{k\to 0}\psi(\mathbf{r}) \propto 1 - \frac{a}{r}, \tag{2.2.5}$$

and

$$f_0(k) = \frac{1}{k\cot\delta_0 - ik} = \frac{\delta_0}{k}. \tag{2.2.6}$$

The scattering length is the intercept of the wave function, given in Eq.(2.2.5), on the r axis as shown in Fig.2.2

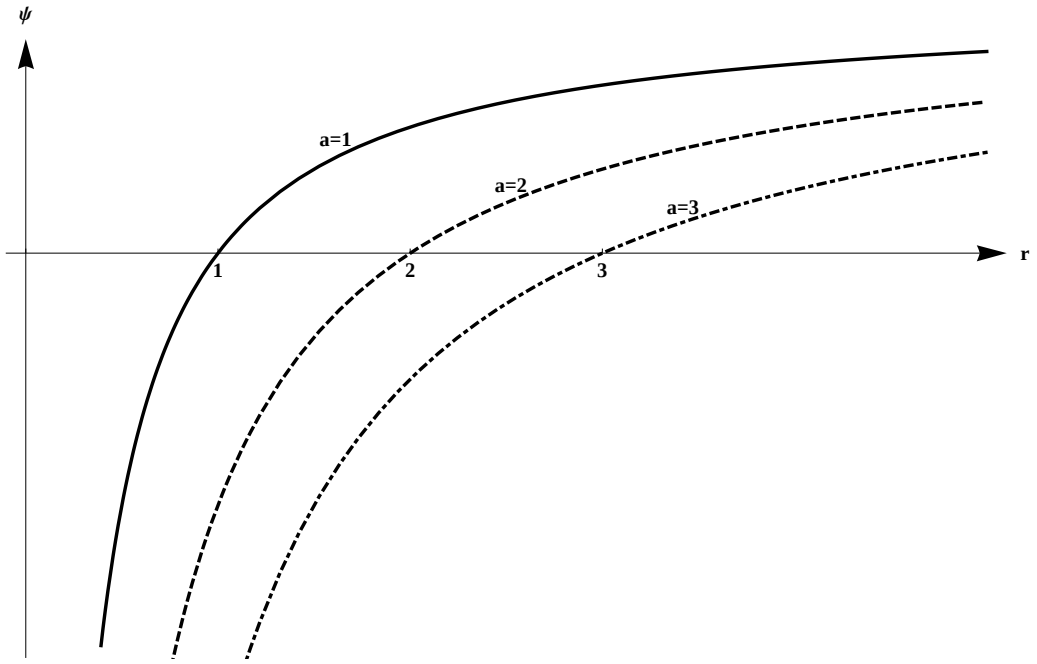

Figure 2.2: *The asymptotic wave function ψ in the low energy limit as a function of r in arbitrary units. The three curves correspond to different values of the scattering length, a=1,2,3. These give the intercept of the wave function on the r axis.*

Using Eq.(2.1.45) and Eq.(2.1.47), the scattering cross section for unlike particles can be expressed as

$$\sigma \sim 4\pi a^2, \tag{2.2.7}$$

and, for identical bosons, as

$$\sigma \sim 8\pi a^2. \tag{2.2.8}$$

However, for identical fermions in the same internal state $\sigma = 0$, the s-wave contact interaction does not contribute due to the Pauli principle.

We need to examine low-energy resonant effects on the scattering length for a single channel. We consider the simple model of the finite spherical square well potential with an attractive part ($V_0 < 0$) and radius r_0 of the form

$$V(r) = \begin{cases} V_0 & \text{if } r < r_0 \\ 0 & \text{if } r > r_0 \end{cases} \tag{2.2.9}$$

Three characteristic length scales that describe a particular aspect of the scattering potential are discussed:

• The *interaction range*, r_0, the distance beyond which the interaction is negligible.

• The $s-wave\ scattering\ length$, a, is defined as the effective hard sphere diameter and determines the collisional cross section and the measure of the interaction strength.

• The $effective\ range$, r_{eff}, shows the energy dependence of the cross section influenced by the potential.

In the following, we express the energy dependence of the s-wave phase shift as a result of the inter-atomic interaction in the presence, and absence, of a weakly bound state for the simplest model potential.

We start by analysing the continuum state for $E > 0$. The corresponding radial Schrödinger equation, obtained from Eq.(2.1.20) by setting $l = 0$ and $u_0 \equiv rR_0(r)$ is

$$u_0''(r) + [\varepsilon - U(r)]\, u_0(r) = 0, \tag{2.2.10}$$

where $\varepsilon = 2\mu E/\hbar^2 = k^2$ and $U(r) = 2\mu V(r)/\hbar^2$.

The solution of Eq.(2.2.10) subjected to boundary conditions is

$$u_0(r) = \begin{cases} A\sin(k_1 r) & \text{if } r \leq r_0 \\ B\sin(kr + \delta_0) & \text{if } r \geq r_0 \end{cases} \tag{2.2.11}$$

The continuity of $u_0(r)$ and $du_0(r)/dr$ at $r = r_0$ requires that

$$k\cot(kr_0 + \delta_0) = k_1 \cot k_1 r_0, \tag{2.2.12}$$

where $k_1 = \sqrt{k_0^2 + k^2}$, and $-k_0^2 = (2\mu/\hbar^2)V_0$. For a vanishing potential at large distances $k_0 \longrightarrow 0$, which implies $k_1 \longrightarrow k$, the boundary conditions in Eq.(2.2.12) becomes

$$k\cot(kr_0 + \delta_0) = k\cot kr_0, \tag{2.2.13}$$

which results in a zero phase shift ($\delta_0 = 0$). In the low-energy limit, ($k \longrightarrow 0$), we might have $k_1 = [k_0^2 + k^2]^{1/2} \longrightarrow k_0$ and from Eq.(2.2.6), $f_0(k) \simeq -a = \delta_0/k$. We expand in first order the l.h.s. of Eq.(2.2.12) and match it with the r.h.s.

$$\begin{aligned} k\cot(kr_0 + \delta_0) &= k\cot(kr_0 - ka) \\ &\simeq \frac{k}{kr_0 - ka} \\ &= k_0 \cot k_0 r_0 \end{aligned} \quad . \tag{2.2.14}$$

We eliminate a to obtain

$$a = r_0 \left(1 - \frac{\tan k_0 r_0}{k_0 r_0}\right), \tag{2.2.15}$$

and the total cross section,

$$\sigma_{tot} \simeq \frac{4\pi}{k^2} \sin^2 \delta_0 \simeq 4\pi r_0^2 \left(\frac{\tan k_0 r_0}{k_0 r_0} - 1\right)^2. \tag{2.2.16}$$

The scattering length can be positive for $k_0 r_0 \gg \pi/2$, negative for $k_0 r_0 \ll \pi/2$ or zero for the values $k_0 r_0 = \tan k_0 r_0$ depending on the depth k_0^2. It can also have the same magnitude as the range of the inter-atomic potential ($a = r_0$). The scattering length and the bound state energy are related. Indeed, for the square well, the *continuum threshold energy* lies just above its bound state energy for a positive and large scattering length as we will see.

For the case of $E < 0$, it turns out that the new bound *s-level* that appears in the square well coincide with the scattering resonant states. We need to solve the Schrödinger equation given by

$$u_0''(r) + [-\varepsilon - U(r)]\, u_0(r) = 0, \tag{2.2.17}$$

where the typical solutions are

$$u_0(r) = \begin{cases} D\sin(k_2 r) & \text{if } r \leq r_0 \\ Ce^{-kr} & \text{if } r \geq r_0 \end{cases} \tag{2.2.18}$$

As previously, the continuity of the solution at $r{=}r_0$ implies

$$-k = k_2 \cot(k_2 r_0), \tag{2.2.19}$$

where $k_2{=}\sqrt{k_0^2 - k^2}$.

We then write the equation for the bound state energy $E_b = -\hbar^2 k^2/2\mu$ as

$$-\sqrt{\frac{2\mu}{\hbar^2}|E_b|} = \sqrt{\frac{2\mu}{\hbar^2}(E_b - V_0)}\cot\left(\sqrt{\frac{2\mu}{\hbar^2}(E_b - V_0)}\right). \tag{2.2.20}$$

The new bound state appears when $k \longrightarrow 0$, which implies $k_2 \longrightarrow k_0$. The above equation (2.2.19) reduces to $k_0 \cot k_0 r_0 = 0$, corresponding to $k_0 r_0 = (n + \frac{1}{2})\pi$. The approximation $-k = k_2 \cot(k_2 r_0) \simeq k_0 \cot k_0 r_0$ holds for weakly bound state.

It follows that

$$-\frac{1}{k} = \frac{\tan k_0 r_0}{k_0}, \tag{2.2.21}$$

so that the scattering length given in Eq.(2.2.15), can be written as

$$a = r_0(1 + \frac{1}{kr_0}) \sim \frac{1}{k} \quad (0 < kr_0 \ll 1). \tag{2.2.22}$$

The scattering length, therefore, becomes *positive* and *large* when there is a weakly bound state with energy given by

$$E_b = -\frac{\hbar^2 k^2}{2\mu} \sim -\frac{\hbar^2}{2\mu a^2}. \tag{2.2.23}$$

We need to give an expression for the effective range. To do so, we apply the angle-addition formula to the tan-function on the r.h.s of Eq.(2.2.12)

$$k \cot(\delta_0 + kr_0) = \frac{k}{\tan(kr_0 + \delta_0)} = \frac{k(1 - \tan kr_0 \tan \delta_0)}{\tan kr_0 + \tan \delta_0}. \tag{2.2.24}$$

By expanding $\tan kr_0$ in (odd) powers of k, an expression for $kr_0 \cot \delta_0(k)$ that contains even powers of k will yield

$$kr_0 \cot \delta_0(k) = \frac{k_1 r_0 \cot k_1 r_0 + k^2 r_0^2 + \cdots}{1 - \left(1 + \frac{1}{3}k^2 r_0^2 + \cdots\right) k_1 r_0 \cot k_1 r_0}. \tag{2.2.25}$$

As seen before, for $k \ll k_0$, $k_1 r_0 = r_0[k_0^2 + k^2]^{1/2} \simeq k_0 r_0 + \frac{1}{2}k^2 r_0^2 / k_0 r_0$. We use the angle-addition formula for the cot-function in $k_1 r_0 \cot k_1 r_0$, so that

$$\begin{aligned} k_1 r_0 \cot k_1 r_0 &= (k_0 r_0 + \frac{1}{2}k^2 r_0^2 / k_0 r_0) \cot(k_0 r_0 + \frac{1}{2}k^2 r_0^2 / k_0 r_0) \\ &= (k_0 r_0 + \frac{1}{2}k^2 r_0^2 / k_0 r_0) \frac{\cot k_0 r_0 \cot(\frac{1}{2}k^2 r_0^2 / k_0 r_0) - 1}{\cot k_0 r_0 + \cot(\frac{1}{2}k^2 r_0^2 / k_0 r_0)}. \end{aligned} \tag{2.2.26}$$

Next, we expand $\cot(\frac{1}{2}k^2 r_0^2 / k_0 r_0)$ in terms of k^2, and after some calculations we find

$$k_1 r_0 \cot k_1 r_0 = \gamma \cot \gamma - \frac{1}{2}k^2 r_0^2 [1 + (1 - \tan \gamma/\gamma) \cot^2 \gamma] \tag{2.2.27}$$

where we have replaced $k_0 r_0$ by the dimensionless parameter γ. The same expansion can also be found in Ref. [49] for the derivation of the effective range. Substituting Eq.(2.2.27) into Eq.(2.2.25), yields

$$kr_0 \cot \delta_0(k) = -\frac{1}{1 - \tan \gamma/\gamma} + \frac{1}{2}k^2 r_0^2 \left(1 - \frac{3(1 - \tan \gamma/\gamma) + \gamma^2}{3\gamma^2 (1 - \tan \gamma/\gamma)^2}\right) + \cdots \tag{2.2.28}$$

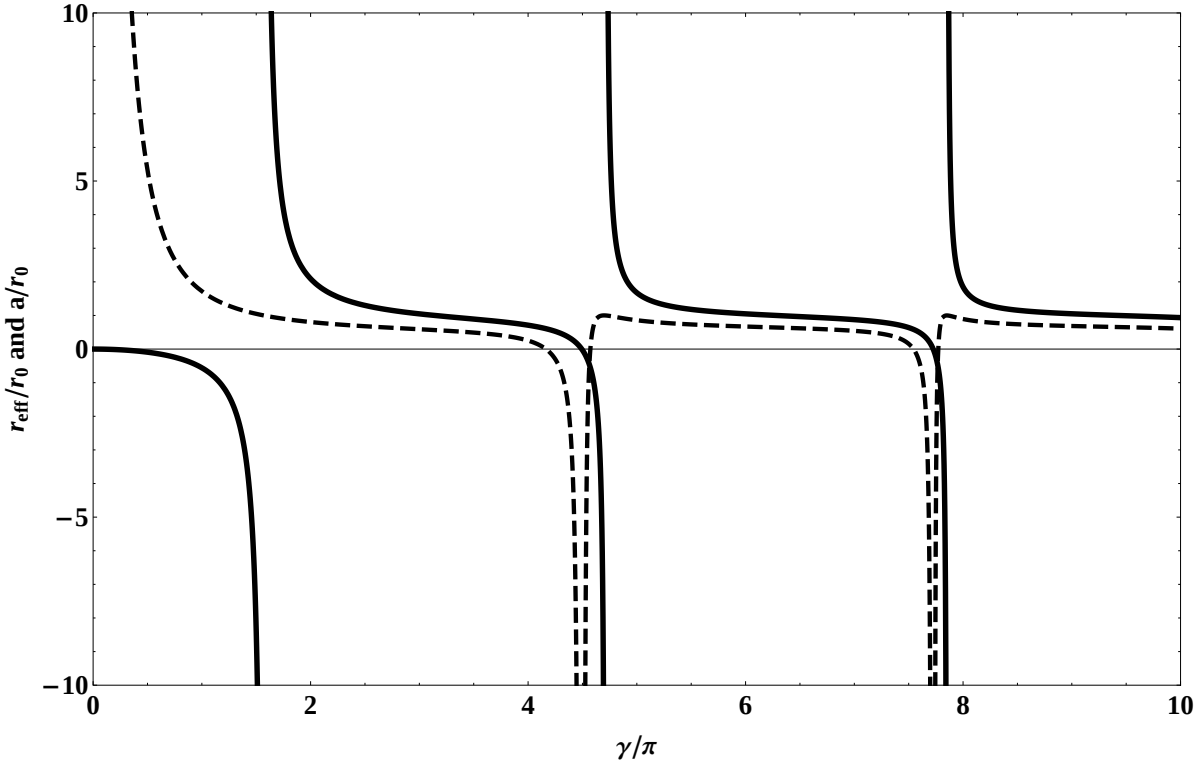

Figure 2.3: *Plots of the scattering length (solid line) and effective range (dashed line) as a function of $k_0 r_0$ for a single model square well potential.*

We have seen from expression (2.2.15) in the low energy limit that $a = r_0(1-\tan\gamma/\gamma)$. The above Eq.(2.2.28) will then reduce to

$$k\cot\delta_0(k) = -\frac{1}{a} + \frac{1}{2}k^2 r_{eff} + \cdots \tag{2.2.29}$$

from which we define the effective range as

$$r_{eff} = r_0\left(1 - \frac{3ar_0 + \gamma^2 r_0^2}{3\gamma^2 a^2}\right). \tag{2.2.30}$$

As shown in Fig.2.3 obtained from Ref. [48], near *resonances* values $k_0 r_0 = (n + \frac{1}{2})\pi$, with n a positive integer, one can see the divergence and change of sign on the scattering length. This behaviour is called *shape* or *potential* resonance and occurs whenever the potential is made deep enough to accommodate a new bound state. From the relation given in Eq.(2.2.30), the effective range diverges for a vanishing scattering length.

Here we have simply given a basic description of a single channel problem of resonances for the elastic scattering in the low energy limit. We have shown the case of a simple model of the spherical square well potential in which we have restricted ourselves to the divergence of the

scattering length (*potential resonance*). We ignore all details regarding resonant enhancement by a weakly bound (s-level) state or virtual state.

Ultimately, the scattering length of an attractive spherical well potential depends largely on the lowest bound state and can take any value, although the relative position of the bound state and the continuum threshold can be tuned by adjusting the shape of the scattering potential. Basically, it is experimentally impossible to change the energy difference between the given bound state and the continuum threshold in the single channel problem. This is due to the fact that, this single potential does not depend on any external parameter.

However, in the multichannel case (next paragraph), we will see that the low energy effective interaction is tunable between atoms experimentally, namely $Fano - Feshbach\ resonances$.

2.2.2 Two-channels scattering problem (Fano-Feshbach resonances)

So far we considered the scattering between spinless cold atoms characterized by a single potential, where atoms scattered elastically. In general, internal states such that electronic and nuclear spins of atoms can affect the scattering process. In the presence of an external magnetic field, the Zeeman splitting of hyperfine levels is observed. We introduce the concept of the *open channel* where atoms are free or far away from each other, and the *closed channel* in which atoms are trapped in a molecular bound state, spending time together before decaying into two separate particles, as illustrated in Fig.2.4. Both channels result from the spin dependence of the interaction between atoms. However, the elastic collisions in the incoming channel can be dramatically affected by the presence of low energy bound states in the closed channel.

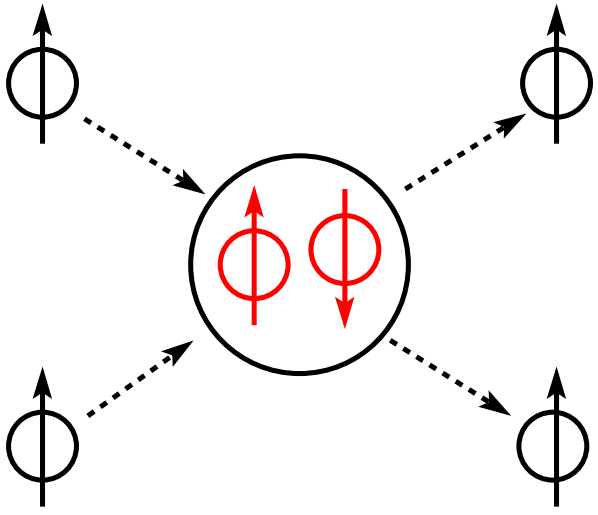

Figure 2.4: *Feshbach resonance of two atomic species colliding with different hyperfine states as indicated by arrows. The two incoming particles are trapped in an intermediate state, spending time together before decaying into free atoms separated from each another.*

Resonance phenomena in nuclear physics are known as *Feshbach Resonances*. The term was introduced in studies of the narrow resonances observed in the total cross section for neutrons scattering of the nucleus [50]. These resonances result from long-lived compound nuclei during collisions. The binding energy of the compound system is close to the energy of the incoming neutrons. In atomic physics they are referred to as *Fano Resonances* where they are at the origin of molecules dissociation and vice versa for bosonic and fermionic atoms [51, 52, 53, 54, 55, 56, 57, 58, 59, 60]. It has been theoretically predicted and observed for different species, as in Ref. [61] and Ref. [62]. The first possibility of magnetically tuning the interactions in the vicinity of Feshbach resonances was discussed by Stwalley with spin-polarized hydrogen and deuterium [63]. For ultracold atomic gases, these resonances are leading tools that enable the tuning of the interactions between atoms and especially the scattering length. For anisotropic interactions between atoms in which atoms collide with non-zero angular momentum (*p-wave* scattering for $l = 1$), Feshbach resonances break up into multiplets due to the magnetic dipole-dipole interaction, as shown in Ref. [64].

2.2.3 Two-body Hamiltonian, Inter-atomic interaction

The starting point is the two-body Hamiltonian that describes the two interacting atoms [65]

$$\hat{H} = \hat{H}_{rel} + \hat{H}_{int}, \tag{2.2.31}$$

where $\hat{H}_{rel} = \mathbf{p}^2/2\mu + V(r)$ stands for the relative motion in the centre of mass frame and $\hat{H}_{int}$ gives the internal energy of the system.

We start by expressing the internal Hamiltonian, $\hat{H}_{int}$, of the colliding atoms as the sum of the hyperfine and the Zeeman interactions. The hyperfine interaction, denoted by $\hat{H}_{hf}$, is caused by the coupling between the nuclear spin and the electronic spin. The Zeeman Hamiltonian, $\hat{H}_z$, arises from the interaction between the magnetic moments of the electrons and the nucleus with an external magnetic field. Thus the Hamiltonian of the internal energy is

$$\hat{H}_{int} = \hat{H}^B_{hf,1} + \hat{H}^B_{hf,2}. \tag{2.2.32}$$

For a single atom α we have,

$$\hat{H}^B_{hf,\alpha} = \hat{H}_{hf,\alpha} + \hat{H}_{z,\alpha} = \frac{a_{hf,\alpha}}{\hbar^2}\mathbf{s}_\alpha \cdot \mathbf{i}_\alpha + \gamma_e \mathbf{B} \cdot \mathbf{s}_\alpha - \gamma_n \mathbf{B} \cdot \mathbf{i}_\alpha \tag{2.2.33}$$

where $\mathbf{s}_\alpha$ and $\mathbf{i}_\alpha$ are electron and nuclear spins. $\mathbf{B}$ is the external magnetic field. The factor a_{hf} is the hyperfine coupling constant, $\gamma_e = g_s\mu_B/\hbar$ and $\gamma_n = g_n\mu_N/\hbar$ are gyromagnetic ratios of the electrons and nucleus. The factors g_e and g_n are known as electronic and nuclear g-factors. μ_B and μ_N are the Bohr and nuclear magneton.
We omitted other weak interactions:
the first is the spin-orbit coupling interaction of the form, $V_{so} = A\mathbf{l} \cdot \mathbf{s}$, which vanishes for $l = 0$.

The second is the magnetic dipole-dipole interaction, $V_{md} = B[\mathbf{s_1}\cdot\mathbf{s_2} - \mathbf{3}(\mathbf{s_1}\cdot\hat{\mathbf{r}})(\mathbf{s_2}\cdot\hat{\mathbf{r}})]/r^3$ between atoms that dominate at large separation. This interaction is much weaker compared to the short range interaction that depends on the spin state of the electrons.

The nuclear and electronic spin add up to the quantum number for the total spin, $\mathbf{f}_\alpha = \mathbf{s}_\alpha + \mathbf{i}_\alpha$, for a single atom α. The hyperfine states are labelled by $|f, m_f\rangle_\alpha$, with m_f the projection of the quantum number f in a particular direction. In the absence of an external magnetic field B, there is no Zeeman splitting of the energy levels. In this case f becomes a good quantum number. So, we have

$$\mathbf{i}\cdot\mathbf{s} = \frac{1}{2}\left[f(f+1) - i(i+1) - s(s+1)\right]. \tag{2.2.34}$$

For alkali and hydrogen atoms in their ground states, as $s = 1/2$, the hyperfine shift of levels $f = i + 1/2$ and $f = i - 1/2$ for a single atom is directly given by

$$\Delta E_{hf} = \frac{a_{hf}}{\hbar^2}(i+s). \tag{2.2.35}$$

For a short range potential $V(r) = 0$ as $r \longrightarrow \infty$, and for sufficient low-energy, the two-body Hamiltonian reduces to $\hat{H}^B_{hf}$ which is independent of r, and the two-body system is described by the eigenstates of each atom individually. The scattering states corresponding to spin states which define the continuum of the system are expressed in the *Breit Rabi* pair basis

$$|f, m_f\rangle_\alpha \otimes |f, m_f\rangle_\beta = |f, m_f\rangle_\alpha |f, m_f\rangle_\beta \tag{2.2.36}$$

that diagonalizes the internal Hamiltonian $\hat{H}^B_{hf}$. The energy level diagram corresponding to molecular states in the system of coupled channels for $(^{40}K - ^{87}Rb)$ is shown in Fig.2.5 obtained from Ref.[66], which contains the colliding continuum energy in $|9/2 - 9/2\rangle|11\rangle$ state and individual hyperfine levels for atoms.

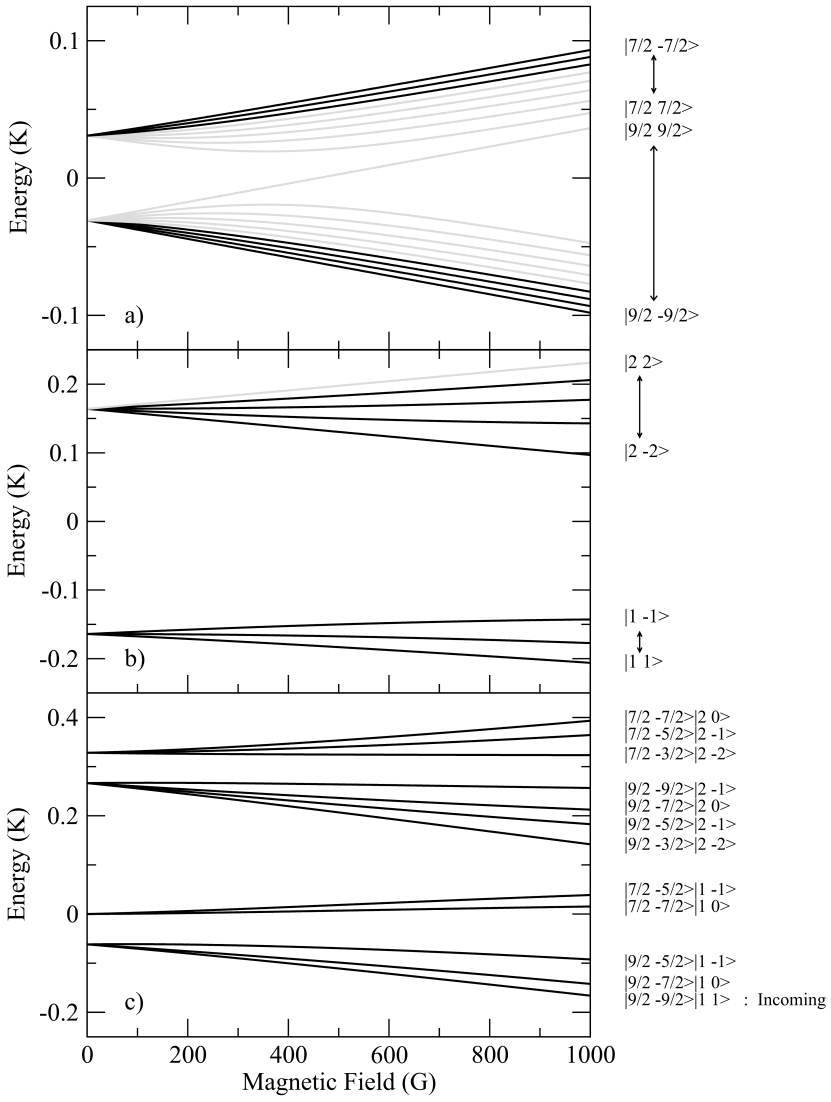

Figure 2.5: *Individual hyperfine states of each atom for:a) K, b) Rb and c) Zeeman splitting of Rb-K hyperfine states in their electronic ground state, including the entrance channel* $|9/2 - 9/2\rangle|1, 1\rangle$

Now let us turn on the effective Hamiltonian that describes the relative motion,

$$\hat{H}_{rel} = \frac{\mathbf{p}^2}{2\mu} + V(r). \tag{2.2.37}$$

Firstly, we need to give the representation of the interatomic interaction V arising from Coulomb interactions between the nuclei and the electrons of the two atoms. Consider two colliding alkali atoms in their electronic ground state. The electronic structure of such atoms is that electrons fill all the inner shells, and the outer shell is occupied by one valence electron (s-shell). As a consequence, the central part of the interaction potential depends on the interatomic position and spins of the two valence electrons of the interacting pair of atoms. Hence, if we neglect the hyperfine interaction, the valence electrons of the two atoms can be either in a triplet state called the *open channel* or singlet state, called the *closed channel*.

The resulting spin for two alkali atoms, $\mathbf{S}$=$\mathbf{s}_\alpha + \mathbf{s}_\beta$ has the basis $|s_\alpha, s_\beta, S, M_S\rangle$ which can be written as $|S, M_S\rangle$. It turns out that for $S \in \{0, 1\}$ and $-S \leq M \leq S$, the singlet state is $|0, 0\rangle$ and the triplet state, $|1, M_S\rangle$. The interaction may be expressed in terms of the product, as described in Ref. [67], as

$$\mathbf{s}_\alpha \cdot \mathbf{s}_\beta = \frac{1}{2}\left[S(S+1) - s_\alpha(s_\alpha+1) - s_\beta(s_\beta+1)\right], \tag{2.2.38}$$

with corresponding eigenvalues in $|s_1, s_2, S, M_S\rangle$ representation -3/4 (singlet states) and 1/4 (triplet states). We can write the spin-dependent interaction in the form

$$V(r) = V_s(r)\mathcal{P}_0 + V_t(r)\mathcal{P}_1 = \frac{V_s(r) + 3V_t(r)}{4} + (V_t(r) - V_s(r))s_\alpha.s_\beta, \tag{2.2.39}$$

where $\mathcal{P}_0 = 1/4 - \mathbf{s}_\alpha \cdot \mathbf{s}_\beta$ and $\mathcal{P}_1 = 3/4 + \mathbf{s}_\alpha \cdot \mathbf{s}_\beta$ are pair electron singlet and triplet projection operators. The plot in Fig.2.6 shows triplet and singlet potential curves responsible for Feshbach resonance as depicted in Ref. [68]. Therefore we see that V_s and V_t representing the singlet and triplet potential are different due to Pauli blocking. Indeed, in singlet state, valence electrons are allowed to be on top of each other because electrons with opposite spin can share the same orbital. Unlike for the triplet state, electrons in the same spin state are forbidden to have the same orbital. The coupling between the external magnetic field $\mathbf{B}$ and the spins will show different

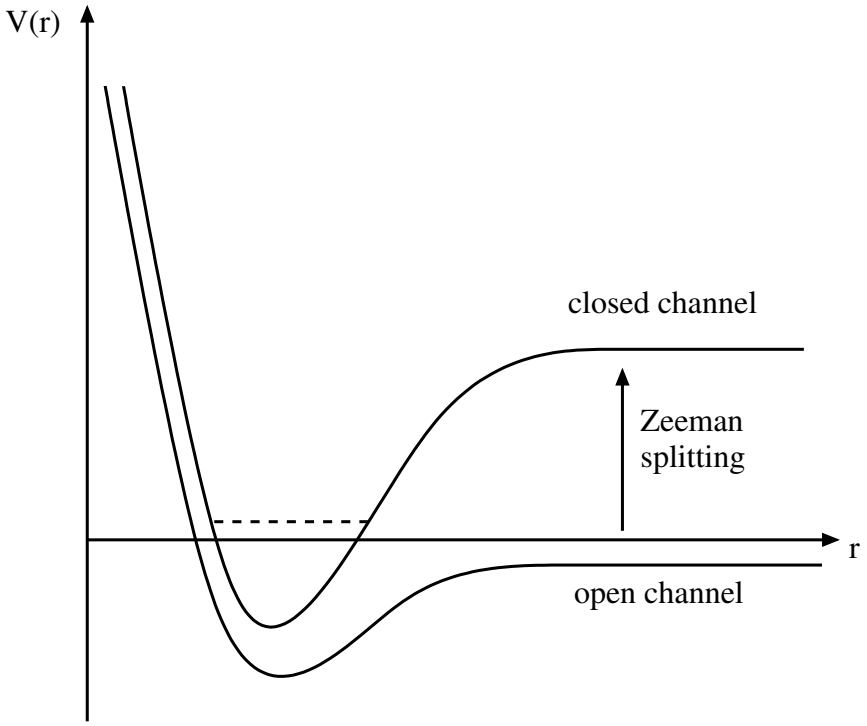

Figure 2.6: *Potential curves representing singlet and triplet potentials. The upper is the closed channel that supports a bound state and it is energetically unfavourable at large separation, while the lower is the open channel, and does not support a bound state because it is much weaker.*

Zeeman splitting for states with non-zero magnetic quantum number M_S for electronic spin. The triplet potential will be shifted down ($M_S = -1$) or up ($M_S = 1$) with respect to the singlet potential. The difference in Zeeman energies are $\Delta E_z = g_s \mu_B B \cdot M_S$ for the electronic spin states and $\Delta E_z = g_n \mu_N B \cdot m_i$ for the nuclear spin states.

2.2.4 Diagonalization of $\hat{H}$ and connection to Feshbach resonance

We will only give an overview on diagonalization procedure of the two-body Hamiltonian, and more details related to the energy levels calculations can be found in Ref. [69]. We search for eigenstates that correspond to molecular hyperfine states and show the connection with Feshbach resonances. Recall that

$$\hat{H} = \hat{H}_{rel} + \hat{H}_{int}. \tag{2.2.40}$$

If there is no coupling between the two potentials (triplet and singlet) due to hyperfine interaction that mixes different spin states, the relative Hamiltonian, written explicitly in terms of eigenvalues of the *angular momentum*, $\mathbf{L} = \mathbf{r} \times \mathbf{p}$ and the *radial momentum*, p_r, is

$$\hat{H}_{rel} = \frac{\hat{p}_r^2}{2\mu} + \frac{l(l+1)\hbar^2}{2\mu r^2} + V(r). \tag{2.2.41}$$

The potential $V(r) = V_s(r)\mathcal{P}_0 + V_t(r)\mathcal{P}_1$ conserves the total orbital angular momentum l due to its rotational invariance in coordinate space. The total electronic spin angular momentum is conserved because it is isotropic in spin space. Then the basis $\{|R_l^S, l, m_l\rangle|s_1, s_2, S, M_S\rangle\}$ diagonalizes $\hat{H}_{rel}$, where $\langle \mathbf{r}|R_l^S, l, m_s\rangle$ can be factorized as a product of radial and angular parts: $R_l^S(r)Y_m^l(\theta, \phi)$.

For given values of s_1, s_2, S and l, the radial wave function $R_{S,l}(r)$, satisfies the Schrödinger equation

$$R''_{S,l} + \frac{2}{r}R'_{S,l} + [\varepsilon - U_{S,l}(r)]\, R_{S,l} = 0 \tag{2.2.42}$$

with $\varepsilon = 2\mu/\hbar^2 E$, the eigenvalue, $U_{S,l}(r) = (2\mu/\hbar^2)\mathcal{V}_{S,l}(r)$ and,

$$\mathcal{V}_{S,l}(r) = V(r) + \frac{l(l+1)\hbar^2}{2\mu r^2} \tag{2.2.43}$$

represents the effective interaction potential.

The solutions of Eq.(2.2.42) that correspond to the continuum threshold ($\varepsilon > 0$) are the wave functions $R_{l,S}(k, r) = \langle r|R_{k,l}^S\rangle$ with the energy

$$\varepsilon_k = k^2. \tag{2.2.44}$$

The corresponding solutions for the bound states ($\varepsilon < 0$) are $R_{v,l,S}(r) = \langle r|R^S_{v,l}\rangle$, defined by their vibrational and rotational quantum numbers v and l for singlet and triplet potentials with binding energies[69]

$$\varepsilon^S_{v,l} = -k^2_{v,S} + l(l+1)\mathcal{R}^S_{v,l}. \tag{2.2.45}$$

The factor $\mathcal{R}^S_{v,l} = \langle R^S_{v,l}|r^{-2}|R^S_{v,l}\rangle$ is called the *rotational constant*.

Indeed, the bound states of the relative Hamiltonian $\hat{H}_{rel}$ will determine the coupled bound states of the effective two-body Hamiltonian $\hat{H}$.

The hyperfine interaction Hamiltonian, $\hat{H}_{hf}$, contained in the internal Hamiltonian $\hat{H}_{int}$ can be written for given particles with spin $s = 1/2$ in terms of two parts, $\hat{H}^+_{hf}$ and $\hat{H}^-_{hf}$ with different symmetry relative to the exchange of nuclear and electron spins, as

$$\hat{H}_{hf} = \hat{H}^+_{hf} + \hat{H}^-_{hf}, \tag{2.2.46}$$

which gives the internal energy $\hat{H}_{int}$

$$\hat{H}_{int} = \hat{H}^+_{hf} + \hat{H}^-_{hf} + \hat{H}_z, \tag{2.2.47}$$

where

$$\hat{H}^\pm_{hf} = \frac{a_{hf1}}{2\hbar^2}(\mathbf{s}_1 \pm \mathbf{s}_2)\cdot\mathbf{i}_1 \pm \frac{a_{hf2}}{2\hbar^2}(\mathbf{s}_1 \pm \mathbf{s}_2)\cdot\mathbf{i}_2, \tag{2.2.48}$$

and

$$\hat{H}_z = \gamma_e\mathbf{B}\cdot(\mathbf{s}_1 + \mathbf{s}_2) - \mathbf{B}\cdot(\gamma_1\mathbf{i}_1 + \gamma_2\mathbf{i}_2). \tag{2.2.49}$$

We note that $\hat{H}^+_{hf}$ contains terms that are proportional to the electronic spin $S = s_\alpha + s_\beta$. It preserves S, but may induce changes in M_S and does not induce singlet-triplet mixing.

$\hat{H}^-_{hf}$, on the other hand does not conserve S which lead to the transformation of singlet states into triplet states and vice versa.

The two-body Hamiltonian can be written as

$$\hat{H} = \hat{H}_{rel} + \hat{H}^+_{hf} + \hat{H}^-_{hf} + \hat{H}_z. \tag{2.2.50}$$

We have seen that the interatomic potential V is diagonal in $|s_\alpha, s_\beta, S, M_S\rangle$ basis but non-diagonal in $|f, m\rangle$ basis, eigenstates of $\hat{H}^B_{hf}$. The consequence is that the internal energies of the system can change during collision and end up in the coupling that gives rise to Feshbach resonances.

To find the eigenvalues relative to binding energies, we have to diagonalize the two-body Hamiltonian $\hat{H}$ in the molecular states basis $\{|R^S_{\upsilon,l}, l, m_l\rangle|s_\alpha, s_\beta, S, M_S\rangle|i_\alpha, i_\beta, m_\alpha, m_\beta\rangle\}$. In this case, by taking into account the orthonormality of the Legendre polynomials $Y^l_m(\theta,\phi)$, we solve the secular equation

$$det|\langle S^{'}, M^{'}_S, m^{'}_1, m^{'}_2|\langle R^{S^{'}}_{\upsilon',l}|\hat{H}_{rel} + \hat{H}^+_{hf} + \hat{H}^-_{hf} + \hat{H}_z - E_b|R^S_{\upsilon,l}\rangle|S, M_S, m_1, m_2\rangle| = 0. \quad (2.2.51)$$

The roots E_b are eigenvalues of $\hat{H}$ that correspond to coupled binding energies. The two-body Hamiltonian defined in Eq.(2.2.50) does not induce any mixing of states with different l and m_l. In fact, it conserves the total angular momentum projection $M_F = M_S + m_1 + m_2$. Consequently, the only non-zero matrix elements are those for $M'_S + m'_1 + m'_2 = M_S + m_1 + m_2$. All terms in $\hat{H}$ are diagonal in the orbital part $|R^S_{\upsilon,l}\rangle$ because they conserve S, except the mixing term $\hat{H}^-_{hf}$.

The matrix elements of $\hat{H}_{rel}$ in molecular basis read

$$\langle S^{'}, M'_{S'}, m'_1, m'_2|\langle R^{S^{'}}_{\upsilon',l}|\hat{H}_{rel}|R^S_{\upsilon,l}\rangle|S, M_S, m_1, m_2\rangle = \varepsilon^S_{\nu,l}\langle R^{S'}_{\nu',l}|R^S_{\nu,l}\rangle\langle S', M'_{S'}, m'_1, m'_2|S, M_S, m_1, m_2\rangle. \quad (2.2.52)$$

For the Zeeman term we have,

$$\langle S^{'}, M'_{S'}, m'_1, m'_2|\langle R^{S^{'}}_{\upsilon',l}|\hat{H}_z|R^S_{\upsilon,l}\rangle|S, M_S, m_1, m_2\rangle = E_z\langle R^{S'}_{\nu',l}|R^S_{\nu,l}\rangle\langle S', M'_{S'}, m'_1, m'_2|S, M_S, m_1, m_2\rangle, \quad (2.2.53)$$

where the Zeeman energy is given by

$$E_z = (\gamma_e M_S - \gamma_1 m_1 - \gamma_2 m_2)B. \quad (2.2.54)$$

The matrix elements of the hyperfine interaction $\hat{H}_{hf} = \hat{H}^+_{hf} + \hat{H}^-_{hf}$ are

$$\langle S^{'}, M'_{S'}, m'_1, m'_2|\langle R^{S^{'}}_{\upsilon',l}|\hat{H}^+_{hf}|R^S_{\upsilon,l}\rangle|S, M_S, m_1, m_2\rangle = \langle R^{S'}_{\nu',l}|R^S_{\nu,l}\rangle\langle S', M'_{S'}, m'_1, m'_2|\hat{H}^+_{hf}|S, M_S, m_1, m_2\rangle, \quad (2.2.55)$$

and

$$\langle S^{'}, M'_{S'}, m'_1, m'_2|\langle R^{S^{'}}_{\upsilon',l}|\hat{H}^-_{hf}|R^S_{\upsilon,l}\rangle|S, M_S, m_1, m_2\rangle = \langle R^{S'}_{\nu',l}|R^S_{\nu,l}\rangle\langle S', M'_{S'}, m'_1, m'_2|\hat{H}^-_{hf}|S, M_S, m_1, m_2\rangle, \quad (2.2.56)$$

Hence for a given value of l, the secular equation takes the form

$$\begin{aligned} det|(\varepsilon^S_{\upsilon,l} - E_b + E_z)\delta_{\upsilon S,\upsilon' S'}\delta_{S,S'}\delta_{M_S,M'_{S'}}\delta_{m_1,m'_1}\delta_{m_2,m'_2} + \delta_{\upsilon,\upsilon'}\langle S', M'_{S'}, m'_1, m'_2|\hat{H}^+_{hf}|S, M_S, m_1, m_2\rangle \\ + \langle R^{S'}_{\nu',l}|R^S_{\nu,l}\rangle\langle S', M'_{S'}, m'_1, m'_2|\hat{H}^-_{hf}|S, M_S, m_1, m_2\rangle| = 0, \end{aligned} \quad (2.2.57)$$

where $\delta_{m_i,m_j} = \langle m_i|m_j\rangle$ and so on for other terms.

Note that the last term in the secular equation, $\langle R^{S'}_{\nu',l}|R^S_{\nu,l}\rangle\langle S', M'_{S'}, m'_1, m'_2|\hat{H}^-_{hf}|S, M_S, m_1, m_2\rangle = 0$ unless $S = S'$.

The terms $\langle R^{S'}_{\nu',l}|R^{S}_{\nu,l}\rangle$ are called $Franck-Condon\ factors$ between different spin states such that $0 \leq |\langle R^{S'}_{\nu',l}|R^{S}_{\nu,l}\rangle| \leq 1$ for $S \neq S'$.

Likewise, the Feshbach resonances appear at magnetic fields for which the orbital of the molecular hyperfine states matches the hyperfine energy of the colliding atoms.

2.2.5 Spherical square wells model for triplet and singlet potentials

We model the triplet and singlet potentials by means of a spherical square well having the same range for convenience as described in Ref. [69, 70] and [71]:

$$V_t(r) = \begin{cases} V_t & \text{if } r \leq r_0 \\ 0 & \text{if } r \geq r_0 \end{cases} \tag{2.2.58}$$

and

$$V_s(r) = \begin{cases} V_s & \text{if } r \leq r_0 \\ \infty & \text{if } r \geq r_0 \end{cases} \tag{2.2.59}$$

where $V_t = -\hbar^2 k_o^2/2\mu$ and $V_s = -\hbar^2 k_c^2/2\mu$. For simplicity we suppose $V_s(r) \longrightarrow \infty$ for $r \geq r_0$. Here $V_t(r)$ is the triplet potential that contains the open s-wave collisional energy $\varepsilon = k^2$ with internal state $|1, M_S\rangle$. $V_s(r)$ is the interacting singlet potential chosen from the asymptote of the triplet potential at $\varepsilon = 0$, with internal state $|0, 0\rangle$. We assume that $V_t < V_s$ such that $V_s(r)$ supports a bound as shown in Fig.2.7 [70]

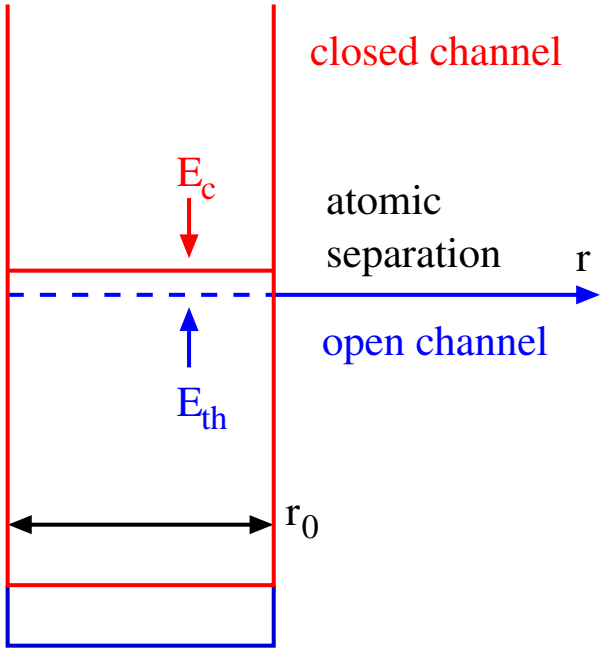

Figure 2.7: *Spherical well representing singlet-triplet potentials. The closed channel contains a bound state relative to the threshold of the open channel.*

In the absence of coupling between channels, the radial wave function solutions for triplet and singlet potentials $V_t(r)$ and $V_s(r)$, including the spin states similar to the case of a single channel problem are, for the open channel,

$$|\psi_t\rangle \approx \frac{\sin k_1 r}{k_1 r}|1, M_S\rangle \qquad \text{if } r < r_0 \tag{2.2.60a}$$

$$|\psi_t\rangle \approx \frac{\sin(kr + \delta_0)}{kr}|1, M_s\rangle \qquad \text{if } r \geq r_0, \tag{2.2.60b}$$

and for the closed channel,

$$|\psi_s\rangle \approx \frac{\sin k_2 r}{k_2 r}|0, 0\rangle \qquad \text{if } r < r_0 \tag{2.2.61a}$$

$$|\psi_s\rangle = 0 \qquad \text{if } r \geq r_0 \tag{2.2.61b}$$

The terms $k_1 = \sqrt{k_o^2 + k^2}$ and $k_2 = \sqrt{k_c^2 + k^2}$ are open and closed channels wave numbers for the relative motion. We note that in the closed channel, the bound state appears whenever $k_2 r_0 = n\pi = q_n r_0$ with binding energies $\varepsilon = q_n^2$ relative to the lowest potential. This is due to the continuity of the solution at $r = r_0$. If there is a coupling between the two potential that we assume to be weak, and denoted by Ω, due to spin mixture between open and closed channels, the interacting potential will become

$$U(r) = -k_o^2|1, M_S\rangle\langle 1, M_S| - k_c^2|0, 0\rangle\langle 0, 0| + \Omega\{|0, 0\rangle\langle 1, M_S| + |1, M_S\rangle\langle 0, 0|\} \tag{2.2.62}$$

for $r < r_0$ and $\infty, 0$ for $r > r_0$. The term Ω, defines the coupling between the channels characterized by their interacting potentials.
The coupling will mix eigenstates of uncoupled Hamiltonians into a new eigenstate $|\psi(r)\rangle$. Consequently, the wave numbers $k_{1,2}$ are shifted to new values $q_{1,2}$. Hence the physics describing the triplet-singlet mixtures can be modelled by the Schrödinger equation

$$\left[\nabla_r^2 + \varepsilon - U(r)\right]|\psi(r)\rangle = 0, \tag{2.2.63}$$

with $U(r) = 2\mu/\hbar^2 V(r)$. The wave function $|\psi(r)\rangle$ which describes the scattering properties of particles in the entrance channel is expressed as a superposition of the triplet and singlet states

$$|\psi(r)\rangle = |\psi_t(r)\rangle + |\psi_s(r)\rangle = \psi_t(r)|1, M_S\rangle + \psi_s(r)|0, 0\rangle, \tag{2.2.64}$$

where $\psi_t(r)$ and $\psi_s(r)$ are triplet and singlet radial wave functions.

In matrix representation we have

$$\begin{pmatrix} \nabla_r^2 + k_o^2 + \varepsilon & -\Omega \\ -\Omega & \nabla_r^2 + k_c^2 + \varepsilon \end{pmatrix} \begin{pmatrix} \psi_t(r) \\ \psi_s(r) \end{pmatrix} = 0. \tag{2.2.65}$$

Here the zero energy for the open channel is chosen as a threshold for dissociation of incoming particles. Since the relative kinetic energy operator is diagonal in the spin space of particles, we seek eigenvalues of the Hamiltonian

$$\hat{H} = \begin{pmatrix} k_o^2 + \varepsilon & -\Omega \\ -\Omega & k_c^2 + \varepsilon \end{pmatrix}. \tag{2.2.66}$$

The eigenvalues are given by

$$\varepsilon_\pm = \varepsilon + \frac{k_o^2 + k_c^2 \pm \sqrt{(k_o^2 - k_c^2)^2 + 4\Omega^2}}{2}. \tag{2.2.67}$$

The canonical transformation that diagonalizes the above Hamiltonian, Eq.(2.2.66), is represented by the following matrix

$$M(\theta) = \begin{pmatrix} \cos\theta & \sin\theta \\ -\sin\theta & \cos\theta \end{pmatrix}, \tag{2.2.68}$$

such that

$$\begin{pmatrix} \varepsilon_- & 0 \\ 0 & \varepsilon_+ \end{pmatrix} = M(\theta)\hat{H}M^{-1}(\theta), \tag{2.2.69}$$

where

$$\cos\theta = \frac{2\Omega}{\sqrt{(k_o^2 - k_c^2 + K)^2 + 4\Omega^2}} \tag{2.2.70a}$$

$$\sin\theta = \frac{k_c^2 - k_o^2 - K}{\sqrt{(k_c^2 - k_o^2 - K)^2 + 4\Omega^2}}, \tag{2.2.70b}$$

with $K^2 = (k_o^2 - k_c^2)^2 + 4\Omega^2$.

We can now define the states $|+\rangle$ and $|-\rangle$ corresponding to spin states of the system

$$|+\rangle = +\cos\theta|1, M_S\rangle + \sin\theta|0, 0\rangle \tag{2.2.71a}$$

$$|-\rangle = -\sin\theta|1, M_S\rangle + \cos\theta|0, 0\rangle. \tag{2.2.71b}$$

Thus the solution of the above Schrödinger equation for the zero scattering energy $\varepsilon = 0$ is given by

$$|\psi(r)\rangle = A_1\frac{\sin q_1 r}{q_1 r}|+\rangle + A_2\frac{\sin q_2 r}{q_2 r}|-\rangle \qquad \text{if } r \le r_0 \tag{2.2.72a}$$

$$|\psi(r)\rangle \simeq \frac{\sin(kr + \delta_0)}{kr}|1, M_S\rangle \qquad \text{if } r \ge r_0, \tag{2.2.72b}$$

where $A_{1,2}$ are constant, to be obtained by the continuity of solutions. The coefficients $q_{1,2}$ are wave numbers related to spin states

$$q_{1,2} = \sqrt{\varepsilon_\pm}. \tag{2.2.73}$$

From these relations, the solution that expresses the effect of the coupling between the two channels for $r < r_0$ will be

$$|\psi(r)\rangle = \left(A_1 \cos\theta \frac{\sin q_1 r}{q_1 r} - A_2 \sin\theta \frac{\sin q_2 r}{q_2 r}\right)|1, M_S\rangle + \left(A_1 \sin\theta \frac{\sin q_1 r}{q_1 r} + A_2 \cos\theta \frac{\sin q_2 r}{q_2 r}\right)|0, 0\rangle. \tag{2.2.74}$$

From the above equation, we can write down the triplet and singlet amplitudes as

$$\psi_t(r) = A_1 \cos\theta \frac{\sin q_1 r}{q_1 r} - A_2 \sin\theta \frac{\sin q_2 r}{q_2 r} \tag{2.2.75a}$$

$$\psi_s(r) = A_1 \sin\theta \frac{\sin q_1 r}{q_1 r} + A_2 \cos\theta \frac{\sin q_2 r}{q_2 r}. \tag{2.2.75b}$$

We can see that both amplitudes are made of two terms $\psi_1(r)$ and $\psi_2(r)$, eigenstates of the coupled system that show the dynamics in space.

The singlet component $\psi_s(r)$ should vanish at $r = r_0$, which implies the condition

$$\frac{A_2}{A_1} = -\frac{q_2 \sin q_1 r_0}{q_1 \sin q_2 r_0} \tan\theta. \tag{2.2.76}$$

Moreover, the continuity of the triplet amplitude $\psi_t(r)$, given in Eq.(2.2.60b) and Eq.(2.2.75b) at $r = r_0$ gives

$$\psi_t(r_0) = \frac{\sin(kr_0 + \delta_0)}{kr_0} = A_1 \left(\cos\theta \frac{\sin q_1 r_0}{q_1 r_0} - \frac{A_2}{A_1} \sin\theta \frac{\sin q_2 r_0}{q_2 r_0}\right), \tag{2.2.77}$$

where the wave number k is associated with the continuum energy in the open channel. Substituting Eq.(2.2.76) into Eq.(2.2.77) will yield the following relation

$$\frac{\sin(kr_0 + \delta_0)}{kr_0} = \frac{\sin q_1 r_0}{q_1 r_0} \frac{A_1}{\cos\theta} = -\frac{\sin q_2 r_0}{q_2 r_0} \frac{A_2}{\sin\theta}. \tag{2.2.78}$$

However, based on the continuity of the logarithmic derivative $\psi_t'(r)/\psi_t(r)$ of the triplet amplitude, and the boundary conditions of $\psi_s(r)$ at $r = r_0$

$$k \cot(kr_0 + \delta_0) = \frac{q_1 \cos^2\theta}{\tan q_1 r_0} + \frac{q_2 \sin^2\theta}{\tan q_2 r_0} = Q_1 + Q_2, \tag{2.2.79}$$

where $Q_1 = q_1 \cos^2\theta / \tan q_1 r_0$ and $Q_2 = q_2 \sin^2\theta / \tan q_2 r_0$.

In the low energy limit, $k \to 0$, the l.h.s of Eq.(2.2.79) compared to Eq.(2.2.15) will reduce to

$$\frac{1}{r_0 - a} = Q_1 + Q_2. \tag{2.2.80}$$

The r.h.s of Eq.(2.2.80) shows how the open and closed channels contribute to the scattering length.

The first term that corresponds to the incoming channel is slightly affected by the outgoing or closed channel via the weak coupling as mentioned before.

The second term that shows the contribution of the closed channel in the limit of weak coupling is small. This term diverges if there is a resonant bound state of energy $E_c = (\hbar^2/2\mu)\varepsilon_c$ in the closed channel relative to the continuum $\varepsilon = k^2$ in the open channel.

The assumptions for the weak coupling, i.e $\Omega \ll k_o^2$, k_c^2 and $|k_o^2 - k_c^2|$, and that $k_o^2 > k_c^2$, imply $\theta \ll 1$ so that

$$\begin{aligned} q_{1,2}^2 &= \varepsilon + \frac{1}{2}\left(k_o^2 + k_c^2 \pm \sqrt{(k_o^2 - k_c^2)^2 + 4\Omega^2}\right) \\ &= \varepsilon + \frac{k_o^2 + k_c^2}{2} \pm \frac{(k_o^2 - k_c^2)}{2}\left(1 + \frac{2\Omega^2}{(k_o^2 - k_c^2)^2} + ++\right) \\ &= \varepsilon + \frac{k_o^2 + k_c^2}{2} \pm \left(\frac{(k_o^2 - k_c^2)}{2} + \frac{\Omega^2}{(k_o^2 - k_c^2)} + ++\right). \end{aligned} \tag{2.2.81}$$

It turns out by comparison with the Eq(2.2.15), we can express the first term in Eq.(2.2.80) as $\cos^2\theta \simeq 1$ and $q_1 \simeq k_o$,

$$Q_1 = q_1 \cos^2\theta \cot q_1 r_0 \equiv k_o \cot k_o r_o \simeq \frac{1}{r_0 - a_{bg}}, \tag{2.2.82}$$

a_{bg} is called the *background scattering length* which in the absence of coupling can be equated to the scattering length in the open channel.
The second term, Q_2, in the limit of weak coupling, as it was shown in Ref.[69] can be approximated to

$$Q_2 = -\frac{\gamma}{\varepsilon_c}, \tag{2.2.83}$$

where $\gamma = 2k_c^2\theta^2/r_0$ represents the *Feshbach coupling stength*.

By substituting Eq.(2.2.82) and Eq.(2.2.83) into Eq.(2.2.80), we obtain the useful relation for the scattering length:

$$\frac{1}{r_0 - a} = \frac{1}{r_0 - a_{bg}} - \frac{\gamma}{\varepsilon_c}. \tag{2.2.84}$$

2.2.6 Magnetic field induced Feshbach resonances

In cold alkali atoms, mostly Feshbach resonances are generated by hyperfine interactions that couples the triplet and singlet states, referred to as the open and closed channels of the two colliding atoms. They appear when the energy of the bound state in the closed channel lies near the threshold continuum of the incoming particles in the open channel. Usually, the corresponding potentials of both channels in the presence of an external magnetic field are shifted with respect to each other, due to the Zeeman effect, with energy $\Delta\mu_B B$. The Zeeman interaction induces the lifting of the degeneracy m_f of the hyperfine levels for particles. Here $\Delta\mu_B$ is the difference in the

magnetic moment of the two channels. Experimentally, Feshbach resonances allow in situ tuning of both the sign and the magnitude of the effective inter-atomic interaction by adjusting linearly a magnetic field, i.e. to alter the scattering length to any desired value. Indeed, by varying the value of the magnetic field, the continuum energy of atoms in the entrance channel will cross the bound state in the closed channel at a given detuning value B_0, converting the binding energy into *energy detuning* of the form

$$\nu = (B - B_0)\Delta\mu_B. \tag{2.2.85}$$

The remaining task is to show the dependence of the scattering length on the magnetic field and the binding energy of the colliding particles.

For cold, alkali atoms, we can see that in the absence of the hyperfine coupling between the two spin states (singlet and triplet), the closed channel binding energy with respect to the triplet channel energy is $E_c = (\hbar^2/\mu)\varepsilon_c$. In the presence of the external homogeneous magnetic field, the energy will be shifted with the Zeeman effect according to

$$E_c(B) = E_c + \Delta\mu_B B, \tag{2.2.86}$$

We substitute the Eq.(2.2.86) into Eq.(2.2.84), which yields

$$\frac{1}{r_0 - a} = \frac{1}{r_0 - a_{bg}} + \frac{B_\gamma}{(r_0 - a_{bg})(B - B_{res})}, \tag{2.2.87}$$

where $B_{res} = -(\hbar^2/\mu)\varepsilon_c/\Delta\mu_B$ is defined as the *resonance field*. The characteristic field $B_\gamma = (\hbar^2/\mu)\gamma(a_{bg} - r_0)/\Delta\mu_B$ shows the *strength* of resonance which is positive for $a_{bg} - r_0 > 0$.

We solve Eq.(2.2.87) for the scattering length a, obtaining

$$a = a_{bg}\left(1 - \frac{\Delta_B}{B - B_0}\right), \tag{2.2.88}$$

where $\Delta_B = (\hbar^2/\mu)\gamma(a_{bg} - r_0)^2/a_{bg}\Delta\mu_B$ characterizes the *width parameter* of the resonance. It can be positive for $a_{bg} - r_0 > 0$. The *apparent Feshbach resonance field* is defined as $B_0 = B_{res} - B_\gamma$.

Eventually, in the weak coupling limit ($B_\gamma \ll B_{res}$), one has

$$a \simeq a_{bg}\left(1 - \frac{\Delta_B}{B - B_{res}}\right). \tag{2.2.89}$$

Equation. (2.2.88) shows explicitly that the scattering length diverges as B become close to B_0, and vanishes when $B - B_0$ approaches the width value Δ_B. It decreases when the resonance

value is crossed by increasing the magnetic field and beyond until the background value $a_{bg} > 0$ is reached as shown in Fig.2.8. But in the case of $a_{bg} < 0$ the inverse process occurs.

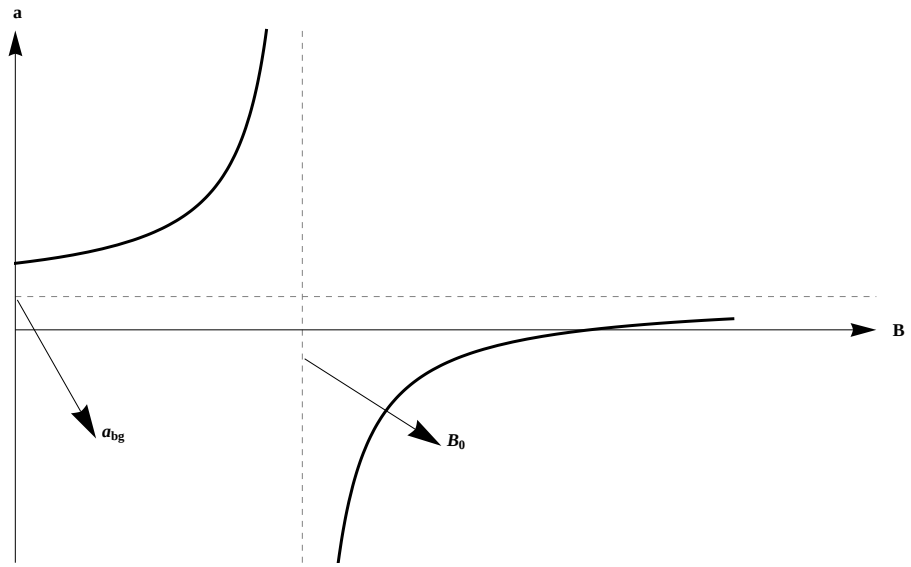

Figure 2.8: *S-wave scattering length behaviour near Feshbach resonance as a function of the magnetic field obtained with current experiments. At the resonance value B_0, there is a divergence.*

Actually, there is a good agreement between the results obtained with current experiments and the theories predicted so far by Feshbach resonances enhanced by a Zeeman shift. Molecular states can be studied, and phase transitions through the implementation of two-body theories such as in the case of Bose-Fermi mixtures of $(^{40}K - ^{87}Rb)$. This is discussed in the next chapter.

Chapter 3

Trapped Bose-Fermi mixtures in The vicinity of Feshbach resonances

In this chapter we analyse the various phases of a resonant Bose-Fermi mixture in a harmonic trap. Contrary to boson-boson and fermion-fermion mixtures where Feshbach molecules are bosons in both cases, here a Feshbach molecule is a fermionic bound state made up of one bosonic and one fermionic atom.
We will use the mean-field approach to investigate the quantum phase transitions of the mixture for a given value of the detuning ν at zero temperature. We will see that at $\nu = 0$, most of the interesting many-body effects characterized by the phase transitions occur in the system.
However, with the presence of the trapping potential which causes the symmetry of the problem to break down, the system becomes inhomogeneous. This renders the calculations very difficult, and we then use the local density approximation (LDA) to map out the phase diagram and density profiles of the various species.

Recent activities on Bose-Fermi mixtures, both experimental and theoretical, have revealed a rich phase structure. The phase transitions can be observed for different values of the detuning ν which depends on the external magnetic field as shown in Ref. [72].

These phase transitions are characterized by the presence or absence of condensed bosons. They are distinguished between them by first-order and second-order phase transition. We also encounter the number of Fermi surfaces changing phases described in Refs. [73, 74, 75]. We will mainly focus on the range where $\nu \geq 0$. The case of $\nu < 0$ will be examine when we analyse the evolution of the population with the global properties of the system. It was shown that in the presence of a condensate, there is a Fermi surface of quasi-particles resulting from the pairing between a boson and a fermion. In the absence of condensed bosons, the Fermi surfaces of free fermions and molecules are distinguishable because the Hamiltonian has a diagonal form.

3.1 Model Hamiltonian

The starting point is the resonant many-body Hamiltonian, as proposed in the case of fermionic atoms [31, 34] to investigate the resonant superfluidity for dilute Fermi gases. The difference lies in the fact that for the mixtures of bosons and fermions, fermionic atoms are treated as spinless particles. We formulate our model in terms of the two-body Hamiltonian that gives the coupling between internal states of atoms. Thus the grand canonical Hamiltonian in second quantized form is given by:

$$\begin{aligned}\hat{H} = \int d\mathbf{x}d\mathbf{y}\Big[&\Psi_b^\dagger(\mathbf{x})T_b(\mathbf{x},\mathbf{y})\Psi_b(\mathbf{y}) + \Psi_f^\dagger(\mathbf{x})T_f(\mathbf{x},\mathbf{y})\Psi_f(\mathbf{y}) + \Psi_m^\dagger(\mathbf{x})T_m(\mathbf{x},\mathbf{y})\Psi_m(\mathbf{y}) \\ &+ \frac{1}{2}\int d\mathbf{x}'d\mathbf{y}'\Psi_b^\dagger(\mathbf{x})\Psi_b^\dagger(\mathbf{y})V(\mathbf{x},\mathbf{y},\mathbf{x}',\mathbf{y}')\Psi_b(\mathbf{y}')\Psi_b(\mathbf{x}') \\ &+ \int d\mathbf{x}'d\mathbf{y}'\Psi_b^\dagger(\mathbf{x})\Psi_f^\dagger(\mathbf{y})V_{bg}(\mathbf{x},\mathbf{y},\mathbf{x}',\mathbf{y}')\Psi_f(\mathbf{y}')\Psi_b(\mathbf{x}') \\ &+ \int d\mathbf{x}'d\mathbf{y}'\left(\Psi_m^\dagger(\frac{\mathbf{x}+\mathbf{y}}{2})g^*(\mathbf{x},\mathbf{y},\mathbf{x}',\mathbf{y}')\Psi_b(\mathbf{y}')\Psi_f(\mathbf{x}') + h.c\right)\Big]\end{aligned} \tag{3.1.1}$$

where

$$\begin{aligned}T_b(\mathbf{x},\mathbf{y}) &= \left(-\frac{\hbar^2\nabla^2}{2m_b} + V_{trap}^b(\mathbf{x}) - \mu_b^0\right)\delta(\mathbf{x}-\mathbf{y}), \\ T_f(\mathbf{x},\mathbf{y}) &= \left(-\frac{\hbar^2\nabla^2}{2m_f} + V_{trap}^f(\mathbf{x}) - \mu_f^0\right)\delta(\mathbf{x}-\mathbf{y}), \\ T_m(\mathbf{x},\mathbf{y}) &= \left(-\frac{\hbar^2\nabla^2}{2\left(m_f+m_b\right)} + V_{trap}^m(\mathbf{x}) + \nu - \mu_m^0\right)\delta(\mathbf{x}-\mathbf{y}),\end{aligned} \tag{3.1.2}$$

are free-evolution operators that describe the dynamics of the non-interacting system.

Here $V_{trap}^b(\mathbf{x})$, $V_{trap}^f(\mathbf{x})$ and $V_{trap}^m(\mathbf{x})$ are the external boson, fermion and molecular trapping potentials. These external atomic trapping potentials are chosen to have the same frequency. It was shown that with current experiments, fermions and bosons experience the same trapping potential [76]. The potential terms that account for non-resonant binary interactions between boson-boson is

$$V(\mathbf{x},\mathbf{y},\mathbf{x}',\mathbf{y}') = V(\mathbf{x}-\mathbf{y})\delta(\mathbf{x}-\mathbf{x}')\delta(\mathbf{y}-\mathbf{y}') \tag{3.1.3}$$

and boson-fermion is

$$V_{bg}(\mathbf{x},\mathbf{y},\mathbf{x}',\mathbf{y}') = V_{bg}(\mathbf{x}-\mathbf{y})\delta(\mathbf{x}-\mathbf{x}')\delta(\mathbf{y}-\mathbf{y}'). \tag{3.1.4}$$

Since we only look at a pure Bose-Einstein condensate and Fermi degenerate gases at zero temperature, we consider only the s-wave terms in the interaction. Therefore we define

$$V(\mathbf{x}-\mathbf{y}) = \frac{4\pi\hbar^2 a_{bb}}{m_b}\delta(\mathbf{x}-\mathbf{y}), \tag{3.1.5}$$

and

$$V_{bg}(\mathbf{x}-\mathbf{y}) = \frac{2\pi\hbar^2 a_{bg}}{m_{bf}}\delta(\mathbf{x}-\mathbf{y}) \tag{3.1.6}$$

that represent the pseudo potentials introduced in Eq.(2.2.4). The factors a_{bb} is the boson-boson s-wave scattering length, and a_{bg} is the boson-fermion background s-wave scattering length.

Finally, the interaction term

$$g(\mathbf{x},\mathbf{y},\mathbf{x}',\mathbf{y}') = g(\mathbf{x}-\mathbf{y})\delta(\mathbf{x}-\mathbf{x}')\delta(\mathbf{y}-\mathbf{y}') \tag{3.1.7}$$

is the coupling potential that combines a boson and a fermion atom into a bound molecular state. Here

$$g(\mathbf{x}-\mathbf{y}) = g\delta(\mathbf{x}-\mathbf{y}), \tag{3.1.8}$$

with

$$g = \sqrt{|V_{bg}|\Delta B\Delta\mu}, \tag{3.1.9}$$

where

$$V_{bg} = \frac{2\pi\hbar^2 a_{bg}}{m_{bf}} \tag{3.1.10}$$

We note that there is no s-wave scattering for identical fermions due to the Pauli principle. $\Psi_b(\mathbf{x})$, $\Psi_f(\mathbf{x})$ and $\Psi_m(\mathbf{x})$ are bosonic atom, fermionic atom and molecular annihilation operators respectively. These operators and their adjoints obey the usual bosonic and fermionic commutation and anticommutation rules such that

$$\left[\Psi_b(\mathbf{x}), \Psi_b^\dagger(\mathbf{y})\right] = \delta(\mathbf{x}-\mathbf{y}), \tag{3.1.11}$$

$$\left\{\Psi_f(\mathbf{x}), \Psi_f^\dagger(\mathbf{y})\right\} = \delta(\mathbf{x}-\mathbf{y}) \tag{3.1.12}$$

and

$$\left\{\Psi_m(\mathbf{x}), \Psi_m^\dagger(\mathbf{y})\right\} = \delta(\mathbf{x}-\mathbf{y}). \tag{3.1.13}$$

The quantities m_b and m_f are the boson and fermion masses, and μ_b^0, μ_f^0 and μ_m^0 are the boson, fermion and molecule chemical potentials.
The detuning that describes the binding energy of molecules as expressed in Eq.(2.2.85) is given by $\nu = (B - B_0)\Delta\mu$.

3.2 Mean-field approach

In this section we need to examine the quantum mechanical formalism of the system through mean-field theory that will allows us to study possible equilibrium properties of the system. As proposed by Bogoliubov for bosonic atoms [77], the mean-field approach to the resonant Bose-Fermi mixtures is obtained by splitting the bosonic field operator in two parts,

$$\Psi_b(\mathbf{x}) = \phi_b(\mathbf{x}) + \delta\Psi_b(\mathbf{x}). \tag{3.2.1}$$

The first term is the expectation value of the boson operator field, $\langle\Psi_b(\mathbf{x})\rangle = \phi_b(\mathbf{x})$. Classically, $\phi_b(\mathbf{x})$ is a ground state wave function describing the bosonic condensate. It is called the order parameter of the phase transition from normal Bose gas to a condensate. The last term $\delta\Psi_b(\mathbf{x})$ is the noncondensed field operator for bosons that described the thermal and quantum fluctuations. This decomposition is crucial since we consider the fraction of noncondensed bosons, or depletion of the condensate, to be very small. This happens for a weakly interacting Bose gas.

By neglecting the fluctuations $\delta\Psi_b(\mathbf{x})$, the mean-field Hamiltonian will read

$$\begin{aligned}\hat{H}_{MF} = \hat{H}(\phi_b) + \int d\mathbf{x}d\mathbf{y}\Big[&\Psi_f^\dagger(\mathbf{x})T_f(\mathbf{x},\mathbf{y})\Psi_f(\mathbf{y}) + \Psi_m^\dagger(\mathbf{x})T_m(\mathbf{x},\mathbf{y})\Psi_m(\mathbf{y}) \\ &+ \int d\mathbf{x'}d\mathbf{y}'\phi_b^*(\mathbf{x})\Psi_f^\dagger(\mathbf{y})V_{bg}(\mathbf{x},\mathbf{y},\mathbf{x}',\mathbf{y}')\Psi_f(\mathbf{y}')\phi_b(\mathbf{x}') \\ &+ \int d\mathbf{x}'d\mathbf{y}'\left\{\Psi_m^\dagger(\frac{\mathbf{x}+\mathbf{y}}{2})g^*(\mathbf{x},\mathbf{y},\mathbf{x}',\mathbf{y}')\phi_b(\mathbf{y}')\Psi_f(\mathbf{x}') + h.c\right\}\Big]\end{aligned} \quad , \tag{3.2.2}$$

where

$$\hat{H}(\phi_b) = \int d\mathbf{x}d\mathbf{y}\left\{\phi_b^*(\mathbf{x})T_b(\mathbf{x},\mathbf{y})\phi_b(\mathbf{y}) + \frac{1}{2}\int d\mathbf{x}'d\mathbf{y}'\phi_b^*(\mathbf{x})\phi_b^*(\mathbf{y})V(\mathbf{x},\mathbf{y},\mathbf{x}',\mathbf{y}')\phi_b(\mathbf{y}')\phi_b(\mathbf{x}')\right\}. \tag{3.2.3}$$

From the mean-field Hamiltonian, the next step is to express the mean value of the energy in terms of densities $\rho_f(\mathbf{x},\mathbf{y}) = \langle\psi_f^\dagger(\mathbf{y})\psi_f(\mathbf{x})\rangle$, $\rho_m(\mathbf{x},\mathbf{y}) = \langle\psi_m^\dagger(\mathbf{y})\psi_m(\mathbf{x})\rangle$, $\rho_{mf}(\mathbf{x},\mathbf{y}) = \langle\psi_f^\dagger(\mathbf{y})\psi_m(\mathbf{x})\rangle$ and $\phi_b(\mathbf{x})$. These densities, which are correlation functions or quantum expectation values with respect to the ground state, describe all physical properties of the Bose-Fermi mixtures.
The mean energy is then

$$\begin{aligned}E(\phi_b,\rho_f,\rho_m,\rho_{mf}) = E(\phi_b) + \int d\mathbf{x}d\mathbf{y}\Big[&T_f(\mathbf{x},\mathbf{y})\rho_f(\mathbf{x},\mathbf{y}) + T_m(\mathbf{x},\mathbf{y})\rho_m(\mathbf{x},\mathbf{y}) \\ &+ \int d\mathbf{x}'d\mathbf{y}'\phi_b^*(\mathbf{x})V_{bg}(\mathbf{x},\mathbf{y},\mathbf{x}',\mathbf{y}')\phi_b(\mathbf{x}')\rho_f(\mathbf{y},\mathbf{y}') \\ &+ \int d\mathbf{x}'d\mathbf{y}'\left\{g^*(\mathbf{x},\mathbf{y},\mathbf{x}',\mathbf{y}')\phi_b(\mathbf{y}')\rho_{fm}(\frac{\mathbf{x}+\mathbf{y}}{2},\mathbf{x}') + h.c\right\}\Big].\end{aligned} \tag{3.2.4}$$

We see that the mean-field Hamiltonian in Eq.(3.2.2) has a quadratic form in creation and annihilation operators. We then proceed with the diagonalization by performing a canonical transformation called Bogoliubov transformation as described in Refs. [78, 79, 80], whereby we write the expansion of the field operators

$$\begin{aligned}\Psi_f(\mathbf{x}) &= \sum_k\left[\alpha_k U_\alpha(k,\mathbf{x}) + \beta_k U_\beta(k,\mathbf{x})\right], \\ \Psi_m(\mathbf{x}) &= \sum_k\left[\alpha_k V_\alpha(k,\mathbf{x}) + \beta_k V_\beta(k,\mathbf{x})\right]\end{aligned}, \tag{3.2.5}$$

where α_k and β_k are quasi-particle fermionic operators that obey the usual fermionic anti-commutation relations

$$\begin{aligned}\left\{\alpha_k^\dagger,\alpha_{k'}\right\} &= \delta_{kk'} \\ \left\{\beta_k^\dagger,\beta_{k'}\right\} &= \delta_{kk'} \\ \left\{\alpha_k^\dagger,\beta_{k'}\right\} &= 0 \\ \left\{\beta_k^\dagger,\alpha_{k'}\right\} &= 0\end{aligned}. \tag{3.2.6}$$

The amplitudes $U_{\alpha,\beta}(k,\mathbf{x})$ and $V_{\alpha,\beta}(k,\mathbf{x})$ are quasi-particle wave functions satisfying the following

conditions for any k,

$$|U_\alpha(k,\mathbf{x})|^2 + |U_\beta(k,\mathbf{x})|^2 = 1 \tag{3.2.7a}$$
$$|V_\alpha(k,\mathbf{x})|^2 + |V_\beta(k,\mathbf{x})|^2 = 1 \tag{3.2.7b}$$
$$U_\beta(k,\mathbf{x}) = V_\alpha(k,\mathbf{x}). \tag{3.2.7c}$$

The completeness relations obtained from the canonical transformation which preserve the anti-commutator relations of the fields $\Psi_f(\mathbf{x})$ and $\Psi_m(\mathbf{x})$ in Eqs.(3.1.12) and (3.1.13) give together with the requirements in Eq.(3.2.6)

$$\sum_k \left[U_{\alpha,\beta}(k,\mathbf{x})U^*_{\alpha,\beta}(k,\mathbf{y}) + V_{\alpha,\beta}(k,\mathbf{x})V^*_{\alpha,\beta}(k,\mathbf{y})\right] = \delta(\mathbf{x}-\mathbf{y}) \tag{3.2.8}$$

and

$$\left\{\Psi_f(\mathbf{x}), \Psi^\dagger_m(\mathbf{y})\right\} = 0 \tag{3.2.9a}$$
$$\sum_k \left[U_\alpha(k,\mathbf{x})U^*_\beta(k,\mathbf{y}) + V_\alpha(k,\mathbf{x})V^*_\beta(k,\mathbf{y})\right] = 0. \tag{3.2.9b}$$

From the inverse transformation

$$\alpha_k = \int d\mathbf{x}\left[U^*_\alpha(k,\mathbf{x})\Psi_f(\mathbf{x}) + V^*_\alpha(k,\mathbf{x})\Psi_m(\mathbf{x})\right] \tag{3.2.10a}$$
$$\beta_k = \int d\mathbf{x}\left[U^*_\beta(k,\mathbf{x})\Psi_f(\mathbf{x}) + V^*_\beta(k,\mathbf{x})\Psi_m(\mathbf{x})\right], \tag{3.2.10b}$$

we obtain the orthogonality conditions for $U_{\alpha,\beta}(k,\mathbf{x})$ and $V_{\alpha,\beta}(k,\mathbf{x})$

$$\left\{\alpha_k, \alpha^\dagger_{k'}\right\} = \delta_{k,k'} \tag{3.2.11a}$$
$$\int \mathrm{d}\mathbf{x}\left[U_{\alpha,\beta}(k,\mathbf{x})U^*_{\alpha,\beta}(k',\mathbf{x}) + V_{\alpha,\beta}(k,\mathbf{x})V^*_{\alpha,\beta}(k',\mathbf{x})\right] = \delta_{k,k'}, \tag{3.2.11b}$$

and

$$\left\{\alpha_k, \beta^\dagger_{k'}\right\} = 0 \tag{3.2.12a}$$
$$\int \mathrm{d}\mathbf{x}\left[U^*_\alpha(k,\mathbf{x})U_\beta(k',\mathbf{x}) + V^*_\alpha(k,\mathbf{x})V_\beta(k',\mathbf{x})\right] = 0. \tag{3.2.12b}$$

For some appropriate choice of $U_{\alpha,\beta}$ and $V_{\alpha,\beta}$ the diagonal form of the mean-field Hamiltonian will be

$$\hat{H}'_{MF} = E_0 + \sum_k \left[\lambda_\alpha \alpha^\dagger_k \alpha_k + \lambda_\beta \beta^\dagger_k \beta_k\right]. \tag{3.2.13}$$

Clearly we can see that $\hat{H}'_{MF}$ is written in terms of free hybrid fermion, quasi-particle excitations α_k and β_k, with dispersion relations $\lambda_{\alpha,\beta} = \lambda_{\alpha,\beta}(k,\mathbf{x})$. We then write down the commutation relations between $\hat{H}'_{MF}$ and the operators α_k and β_k to obtain

$$\begin{aligned}\left[\alpha_k, \hat{H}'_{MF}\right] &= \lambda_\alpha \alpha_k \\ \left[\beta_k, \hat{H}'_{MF}\right] &= \lambda_\beta \beta_k\end{aligned}. \tag{3.2.14}$$

To derive equations for the quasi-particle amplitudes $U_{\alpha,\beta}(k,\mathbf{x})$ and $V_{\alpha,\beta}(k,\mathbf{x})$, we calculate the commutators

$$\left[\Psi_f(\mathbf{x}),\hat{H}'_{MF}\right] = \sum_k \left[\lambda_\alpha U_\alpha(k,\mathbf{x})\alpha_k + \lambda_\beta V_\alpha(k,\mathbf{x})\beta_k\right] \tag{3.2.15a}$$

$$\left[\Psi_f(\mathbf{x}),\hat{H}_{MF}\right] = \int d\mathbf{y}\left[h_f(\mathbf{x},\mathbf{y})\Psi_f(\mathbf{y}) + \Delta(\mathbf{x},\mathbf{y})\Psi_m(\mathbf{y})\right]. \tag{3.2.15b}$$

$$\left[\Psi_m(\mathbf{x}),\hat{H}'_{MF}\right] = \sum_k \left[\lambda_\alpha U_\beta(k,\mathbf{x})\alpha_k + \lambda_\beta V_\beta(k,\mathbf{x})\beta_k\right] \tag{3.2.16a}$$

$$\left[\Psi_m(\mathbf{x}),\hat{H}_{MF}\right] = \int d\mathbf{y}\left[h_m(\mathbf{x},\mathbf{y})\Psi_m(\mathbf{y}) + \Delta^*(\mathbf{x},\mathbf{y})\Psi_f(\mathbf{y})\right]. \tag{3.2.16b}$$

We define the expressions

$$\begin{aligned} h_f(\mathbf{x},\mathbf{y}) = \frac{\delta E(\phi_b,\rho_f,\rho_m,\rho_{mf})}{\delta\rho_f(\mathbf{x},\mathbf{y})} &= T_f(\mathbf{x},\mathbf{y}) + \int d\mathbf{x}'d\mathbf{y}'\phi_b^*(\mathbf{y}')V_{bg}(\mathbf{x},\mathbf{y},\mathbf{x}',\mathbf{y}')\phi_b(\mathbf{x}') \\ h_m(\mathbf{x},\mathbf{y}) = \frac{\delta E(\phi_b,\rho_f,\rho_m,\rho_{mf})}{\delta\rho_m(\mathbf{x},\mathbf{y})} &= T_m(\mathbf{x},\mathbf{y}) \end{aligned}, \tag{3.2.17}$$

as single-particle potentials for fermions and molecules.
The coupling field similar to the BCS (Bardeen-Cooper-Schrieffer) gap parameter in the case of a two-component Fermi gas [34] is defined by

$$\Delta(\mathbf{x},\mathbf{y}) = \int d\mathbf{x}'d\mathbf{y}' g(\mathbf{x},\mathbf{y},\mathbf{x}',\mathbf{y}')\phi_b^*(\mathbf{y}') \tag{3.2.18}$$

We replace the fields $\Psi_f(\mathbf{y})$ and $\Psi_m(\mathbf{y})$ on the r.h.s. of Eqs.(3.2.15b) and (3.2.16b) by their expansions given in Eq.(3.2.5) to obtain

$$\begin{aligned} \left[\Psi_f(\mathbf{x}),\hat{H}_{MF}\right] = \sum_k \int d\mathbf{y}\Big(& h_f(\mathbf{x},\mathbf{y})\alpha_k U_\alpha(k,\mathbf{y}) + h_f(\mathbf{x},\mathbf{y})\beta_k U_\beta(k,\mathbf{y}) \\ &+ \Delta(\mathbf{x},\mathbf{y})\alpha_k V_\alpha(k,\mathbf{y}) + \Delta(\mathbf{x},\mathbf{y})\beta_k V_\beta(k,\mathbf{y})\Big) \end{aligned} \tag{3.2.19}$$

$$\begin{aligned} \left[\Psi_m(\mathbf{x}),\hat{H}_{MF}\right] = \sum_k \int d\mathbf{y}\Big(& h_m(\mathbf{x},\mathbf{y})\alpha_k V_\alpha(k,\mathbf{y}) + h_m(\mathbf{x},\mathbf{y})\beta_k V_\beta(k,\mathbf{y}) \\ &+ \Delta^*(\mathbf{x},\mathbf{y})\alpha_k U_\alpha(k,\mathbf{y}) + \Delta^*(\mathbf{x},\mathbf{y})\beta_k U_\beta(k,\mathbf{y})\Big). \end{aligned} \tag{3.2.20}$$

For each value of k, we compare the coefficients α_k and β_k by equating Eq.(3.2.15a) with Eq.(3.2.19) and Eq.(3.2.16a) with Eq.(3.2.20). This will result in the Harthree-Fock-Bogoliubov (HFB) like equations for the quasi-particle amplitudes ($U_{\alpha,\beta}(k,\mathbf{x})$ and $V_{\alpha,\beta}(k,\mathbf{x})$

$$\lambda_{\alpha,\beta}U_{\alpha,\beta}(k,\mathbf{x}) = \int d\mathbf{y}\left[h_f(\mathbf{x},\mathbf{y})U_{\alpha,\beta}(k,\mathbf{y}) + \Delta(\mathbf{x},\mathbf{y})V_{\alpha,\beta}(k,\mathbf{y})\right] \tag{3.2.21a}$$

$$\lambda_{\alpha,\beta}V_{\alpha,\beta}(k,\mathbf{x}) = \int d\mathbf{y}\left[\Delta^*(\mathbf{x},\mathbf{y})U_{\alpha,\beta}(k,\mathbf{y}) + h_m(\mathbf{x},\mathbf{y})V_{\alpha,\beta}(k,\mathbf{y})\right]. \tag{3.2.21b}$$

3.3 Local density approximation (LDA)

In order to describe the inhomogeneity of the system due by the trapping potential, we consider the gas in the Thomas-Fermi approximation, also called the local density approximation (LDA) [73]. We assume the particles to be trapped in a uniform potential, with slowly varying spacial density so that each point of space is treated locally. It is now convenient to define all quantities as functions of the centre of mass position $\mathbf{R}$ in the trap and the relative momentum $\mathbf{k}$. This was done in Refs. [34, 81, 82], where it was suggested the quasi-particle amplitudes to be of the form

$$\begin{pmatrix} U_{\alpha,\beta}(\mathbf{k},\mathbf{x}=\mathbf{R}\pm\mathbf{r}/2) \\ V_{\alpha,\beta}(\mathbf{k},\mathbf{x}=\mathbf{R}\pm\mathbf{r}/2) \end{pmatrix} = \begin{pmatrix} U_{\alpha,\beta}(\mathbf{k},\mathbf{R}) \\ V_{\alpha,\beta}(\mathbf{k},\mathbf{R}) \end{pmatrix} \exp(i\mathbf{k}\cdot\mathbf{x}). \tag{3.3.1}$$

After substitution of the Fourier components of the amplitudes given in Eq.(3.3.1), we neglect the gradient over density because the kinetic energy of the gas is sufficiently low. The set of equations in Eq.(3.2.21a) and Eq.(3.2.21b), for every quasi-particle with momentum k, will become similar to the local Bogoliubov-de-Gennes equations [80] with an additional term for the bosonic field.

$$\lambda_{\alpha,\beta}(k,\mathbf{R})U_{\alpha,\beta}(k,\mathbf{R}) = h_f(k,\mathbf{R})U_{\alpha,\beta}(k,\mathbf{R}) + \Delta(\mathbf{R})V_{\alpha,\beta}(k,\mathbf{R}) \tag{3.3.2a}$$

$$\lambda_{\alpha,\beta}(k,\mathbf{R})V_{\alpha,\beta}(k,\mathbf{R}) = \Delta^*(\mathbf{R})U_{\alpha,\beta}(k,\mathbf{R}) + h_m(k,\mathbf{R})V_{\alpha,\beta}(k,\mathbf{R}). \tag{3.3.2b}$$

Finally, we get two eigenvalues that represent the local dispersion relations of mixed quasi-fermions after solving Eq (3.3.2a) and Eq.(3.3.2b)

$$\lambda_{\alpha,\beta}(k,\mathbf{R}) = \frac{h_f(k,\mathbf{R}) + h_m(k,\mathbf{R})}{2} \pm \frac{1}{2}\sqrt{4|\Delta(\mathbf{R})|^2 + (h_m(k,\mathbf{R}) - h_f(k,\mathbf{R}))^2}. \tag{3.3.3}$$

The elements of the unitary matrix are

$$U_\alpha(k,\mathbf{R}) = \frac{2\Delta(\mathbf{R})}{\sqrt{(h_m(k,\mathbf{R}) - h_f(k,\mathbf{R}) + K(k,\mathbf{R}))^2 + 4\Delta(\mathbf{R})^2}}, \tag{3.3.4a}$$

$$V_\alpha(k,\mathbf{R}) = \frac{h_m(k,\mathbf{R}) - h_f(k,\mathbf{R}) + K(k,\mathbf{R})}{\sqrt{(h_m(k,\mathbf{R}) - h_f(k,\mathbf{R}) + K(k,\mathbf{R}))^2 + 4\Delta(\mathbf{R})^2}}, \tag{3.3.4b}$$

$$U_\beta(k,\mathbf{R}) = \frac{h_f(k,\mathbf{R}) - h_m(k,\mathbf{R}) - K(k,\mathbf{R})}{\sqrt{(h_f(k,\mathbf{R}) - h_m(k,\mathbf{R}) - K(k,\mathbf{R}))^2 + 4\Delta(\mathbf{R})^2}}, \tag{3.3.4c}$$

$$V_\beta(k,\mathbf{R}) = \frac{2\Delta(\mathbf{R})}{\sqrt{(h_f(k,\mathbf{R}) - h_m(k,\mathbf{R}) - K(k,\mathbf{R}))^2 + 4\Delta(\mathbf{R})^2}}, \tag{3.3.4d}$$

where

$$K(k,\mathbf{R}) = \sqrt{4|\Delta(\mathbf{R})|^2 + (h_m(k,\mathbf{R}) - h_f(k,\mathbf{R}))^2}. \tag{3.3.5}$$

We choose $\lambda_\alpha(k,\mathbf{R}) \geq \lambda_\beta(k,\mathbf{R})$.
The terms

$$h_f(k,\mathbf{R}) = \frac{\hbar^2 k^2}{2m_f} - \mu_f(\mathbf{R}) + V_{bg}\rho_b(\mathbf{R}), \tag{3.3.6}$$

and

$$h_m(k,\mathbf{R}) = \frac{\hbar^2 k^2}{2(m_f + m_b)} - \mu_b(\mathbf{R}) - \mu_f(\mathbf{R}) + \nu \tag{3.3.7}$$

are local single-particle potentials.
We define

$$\mu_{b,f}(\mathbf{R}) = \mu^0_{b,f} - V^{b,f}_{trap}(\mathbf{R}) \tag{3.3.8}$$

as the local chemical potentials, and

$$\Delta(\mathbf{R}) = g\sqrt{\rho_b(\mathbf{R})}, \tag{3.3.9}$$

expresses the local coupling term.
The term

$$\rho_b(\mathbf{R}) = |\phi_b(\mathbf{R})|^2 \tag{3.3.10}$$

represents the density of condensed bosons.

The remaining task is to find physical quantities such as the density of each species in the system that will allow us to compute the phase diagram of the mixtures. We start first by expressing local distributions $\rho_f(k,\mathbf{R})$, $\rho_m(k,\mathbf{R})$ and $\rho_{fm}(k,\mathbf{R})$ in terms of the quasi-particle basis. We know that the quasi-particle basis at equilibrium is filled up following the Fermi distributions $n_{\alpha,\beta}(k,\mathbf{R}) = (exp(\lambda_{\alpha,\beta}(k,\mathbf{R})/k_BT) + 1)^{-1}$, i.e.

$$\langle \alpha^\dagger_k \alpha_{k'} \rangle = \delta_{kk'} n_\alpha(k,\mathbf{R}), \tag{3.3.11}$$

and

$$\langle \beta^\dagger_k \beta_{k'} \rangle = \delta_{kk'} n_\beta(k,\mathbf{R}). \tag{3.3.12}$$

Since we are looking at a zero-temperature phase diagram, the Fermi distribution reduces to the step function,

$$n_{\alpha,\beta}(k,\mathbf{R}) = \Theta(-\lambda_{\alpha,\beta}(k,\mathbf{R})). \tag{3.3.13}$$

The distributions $n_{\alpha,\beta}(k,\mathbf{R})$ define the local Fermi wave number $k^0_{\alpha,\beta}(\mathbf{R})$ from which $\lambda_{\alpha,\beta}(k,\mathbf{R}) \leq 0$. This will allow to find the number of Fermi surfaces which disappear when $k^0_{\alpha,\beta}(\mathbf{R})$=0

We then obtain the following relations for distributions in the quasi-particle basis

$$\rho_f(k,\mathbf{R}) = \langle \Psi^\dagger_f(k,\mathbf{R})\Psi_f(k,\mathbf{R})\rangle = |U_\alpha(k,\mathbf{R})|^2 n_\alpha(k,\mathbf{R}) + |V_\alpha(k,\mathbf{R})|^2 n_\beta(k,\mathbf{R}), \tag{3.3.14}$$

$$\rho_m(k,\mathbf{R}) = \langle \Psi^\dagger_m(k,\mathbf{R})\Psi_m(k,\mathbf{R})\rangle = |U_\beta(k,\mathbf{R})|^2 n_\alpha(k,\mathbf{R}) + |V_\beta(k,\mathbf{R})|^2 n_\beta(k,\mathbf{R}), \tag{3.3.15}$$

and

$$\rho_{mf}(k,\mathbf{R}) = \langle \Psi^\dagger_f(k,\mathbf{R})\Psi_m(k,\mathbf{R})\rangle = U^*_\alpha(k,\mathbf{R})U_\beta(k,\mathbf{R})n_\alpha(k,\mathbf{R}) + V^*_\alpha(k,\mathbf{R})V_\beta(k,\mathbf{R})n_\beta(k,\mathbf{R}). \tag{3.3.16}$$

The local densities of species in the system are expressed as

$$\rho_f(\mathbf{R}) = \int \frac{d^3k}{(2\pi)^3}\rho_f(k,\mathbf{R}), \tag{3.3.17}$$

$$\rho_m(\mathbf{R}) = \int \frac{d^3k}{(2\pi)^3}\rho_m(k,\mathbf{R}) \tag{3.3.18}$$

and

$$\rho_{mf}(\mathbf{R}) = \int \frac{d^3k}{(2\pi)^3}\rho_{mf}(k,\mathbf{R}). \tag{3.3.19}$$

3.4 Characterization of phase transitions

From thermodynamics, one makes use of the free energy as an ingredient to obtain all properties of the system. Indeed, the global ($\rho_b = \rho_{min}$) minima of the free energy which describe the states with lowest energy define the stability of the system. Those minima are called order parameters according to the Landau theory of phase transitions. The order parameter is obtained when we minimize the local free energy with respect to bosonic density ρ_b.

We characterize the phase transitions from zero condensate ($\rho_{min} = 0$) to non-zero ($\rho_{min} \neq 0$) in terms of its order. Therefore we need to study the global minima of the local ground state energy for a given ρ_b. The energy density is obtained from Eq.(3.2.4) after solving for $\rho_f(k,\mathbf{R})$, $\rho_m(k,\mathbf{R})$, $\rho_{mf}(k,\mathbf{R})$ and $\rho_b(\mathbf{R})$, namely

$$\begin{aligned} E(\mathbf{R}) = &-\mu_b(\mathbf{R})|\phi_b(\mathbf{R})|^2 + \frac{1}{2}V|\phi_b(\mathbf{R})|^4 \\ &+ \int \frac{d^3k}{(2\pi)^3}\left[h_f(k,\mathbf{R})\rho_f(k,\mathbf{R}) + h_m(k,\mathbf{R})\rho_m(k,\mathbf{R})\right] \\ &+ \int \frac{d^3k}{(2\pi)^3}\left[g^*\rho_{mf}(k,\mathbf{R})\phi_b(\mathbf{R}) + g\rho_{fm}(k,\mathbf{R})\phi_b^*(\mathbf{R})\right]. \end{aligned} \tag{3.4.1}$$

The first two terms in Eq.(3.4.1) give the classical behaviour and has a positive global minimum at $\rho_b = |\phi_b(\mathbf{R})|^2 = \mu_b(\mathbf{R})/V$ for $\mu_b > 0$. The last terms contribute to the appearance of the local minimum that describes the phase transition in the system, even for a negative bosonic chemical potential.

All expressions are calculated at the equilibrium density of condensed bosons, ρ_{min}, resulting from the global minimum of the energy $E(\mathbf{R})$. This minimum ρ_{min}, corresponding to the lowest value of the energy density $E(\rho_{min})$, is the root of the derivative

$$\frac{\delta E}{\delta \rho_b} = \left(-\mu_b(\mathbf{R}) + V_{bg}\rho_f(\mathbf{R})\right)\sqrt{\rho_b(\mathbf{R})} + V\rho_b^{3/2}(\mathbf{R}) + g\rho_{fm}(\mathbf{R}). \tag{3.4.2}$$

If the global minimum of the energy density presents a jump of discontinuity, the system undergoes the first order phase transition. If it is continuous, we are dealing with the second order phase transition.

To explore the quantum phase transitions in terms of parameters such as chemical potentials μ_b and μ_f, interacting terms V, V_{bg} and g and the detuning ν, we need to rescale quantities such as the densities and the energy of the system. We choose an arbitrary number of free fermions, $N_f = 10^6$, confined in an harmonic trapping potential with axial frequency $100Hz$. All quantities that have the dimension of energy need to be compared with the free arbitrary Fermi energy $E_f = \omega(6\lambda N_f)^{1/3}$ of the trap as a unit. The asymmetry parameter $\lambda = \omega_z/\omega_\perp$ represents the trap aspect ratio of the transverse and axial frequencies. The densities of species are compared with the cube of the arbitrary Fermi wave number, k_f^3.

We write all parameters in dimensionless form and use the same parametrization of the Feshbach resonances for the magnetic field $B_0 = 492.49G$ as was done in Ref. [83]. Which follow by writing $\tilde{\mu}_b = \mu_b/E_f$ and $\tilde{\mu}_f = \mu_f/E_f$, $\tilde{V} = Vk_f^3/E_f$, $\tilde{V}_{bg} = V_{bg}k_f^3/2E_f$, $\tilde{g} = \sqrt{V_{bg}\Delta B\Delta\mu}k_f^{3/2}/2E_f$ and $\tilde{\nu} = \nu/E_f$. These parametrization is useful for the comparison with experiments. All values are listed in the table. We choose the scattering lengths a_{bb}, related to boson-boson interactions to

Physical Quantity	Value $(a.u.)$
B_0	492.49
ΔB	0.134
$\Delta\mu_B$	$3.624\times10^{-5}/(3.157\times10^{5})$
ω	$100\times2.41889\times10^{-17}$
m_{Rb}	87×1822
m_K	40×1822
a_{bg}	-179.5
a_{bb}	109
λ	0.5
$\hbar$	1

Table 3.1: *Physical quantities used for numerical simulations in this thesis*

be positive and a_{bg}, related to boson-fermion interactions to be negative. The choice of $a_{bg} < 0$ contributes to the mechanical stability of the system, as described in Ref. [84] page. The positive value of a_{bb} is adequate to maintain the system thermodynamically stable.
Since the interaction between bosons is repulsive, as explained in Ref. [40], the molecules will induce bosons-attractive interactions that will overcome boson-fermion attractions leading to more condensed bosons. This effect will lower the energy of the system. If the interaction between bosons were attractive, the mixture would be unstable due to the collapse of bosons.

Usually, two different phase transitions take place with a Bose-Einstein condensate in the presence of a Fermi degenerate gas. One occurs when the (local) minimum in the energy density goes from zero to a nonzero value discontinuously. This happens when we move around the plane of local chemical potential. The phenomenon is called the first-order phase transition and takes place at the point where $E(\rho_{min} = 0)$ coincides with $E(\rho_{min} \neq 0)$. Figure 3.1 gives a good illustration of the first-order phase transition in Bose-Fermi mixtures. Figure 3.2 shows the behaviour of the energy around the first-order phase transition where it develops its second minimum at $\rho_{min} > 0$.

As the minimum, ρ_{min}, presents a jump of discontinuity, particle densities that are calculated at this point are also discontinuous around the first-order phase transition line.

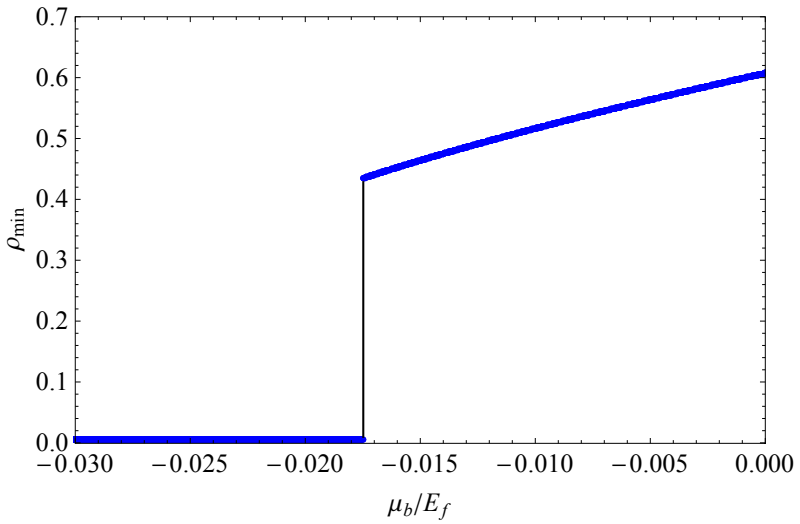

Figure 3.1: *Plot of the local minimum of the energy as a function of local μ_b, for a given value of local μ_f. We see the jump of discontinuity characterizing the first-order phase transition.*

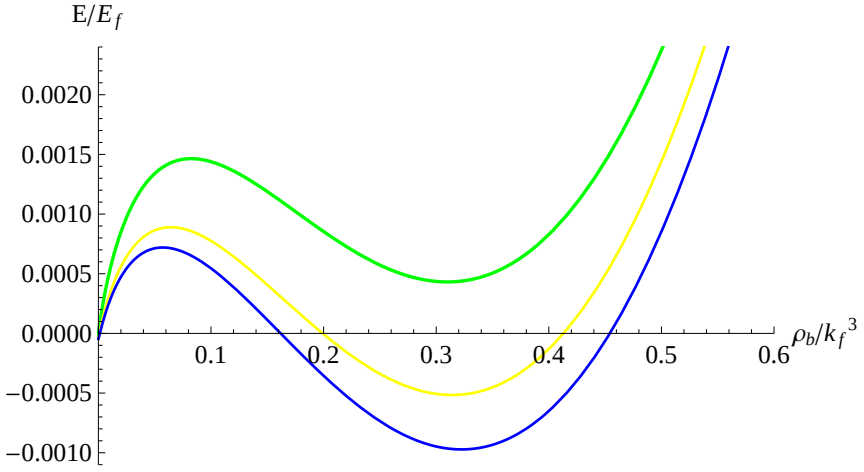

Figure 3.2: *Plot of the free energy as a function of ρ_b showing the first-order phase transition for the Bose-Fermi mixture as we move around in the plane of local chemical potentials where the local minimum undergoes a jump of discontinuity from $\rho_{min} = 0$ to $\rho_{min} \neq 0$. The curves correspond, from the top to the bottom to values of μ_b/E_f=-0.1196, -0.1276 and -0.1286 and μ_f/E_f=0.0802, 0.265 and 0.1360.*

The second transition is called the second-order phase transition. It arises when the minimum of the energy density changes from zero to a nonzero value continuously, as shown in Fig.3.3. Figure 3.4 gives the behaviour of the energy for the second-order phase transition. In this case particle densities are continuous as we move away from the center of the trap.

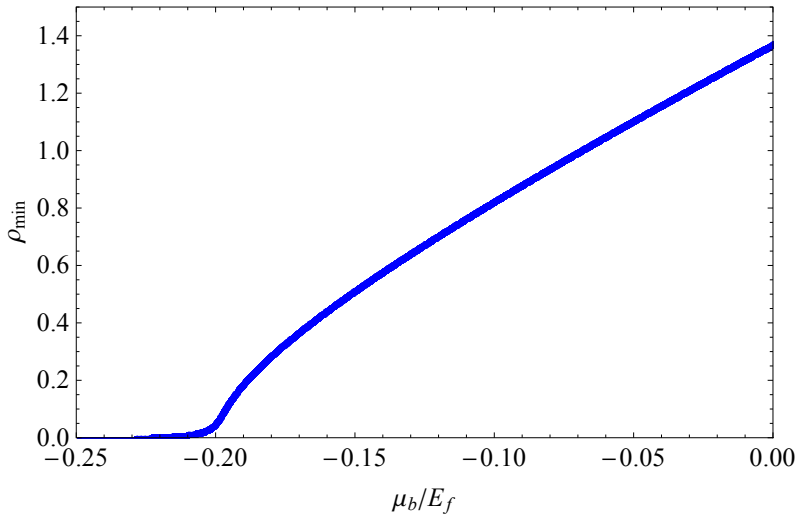

Figure 3.3: *Plot of the local minimum of the energy as a function of the local μ_b/E_f for a given value of μ_f/E_f. The continuity of the local minimum here characterizes the second-order phase transition.*

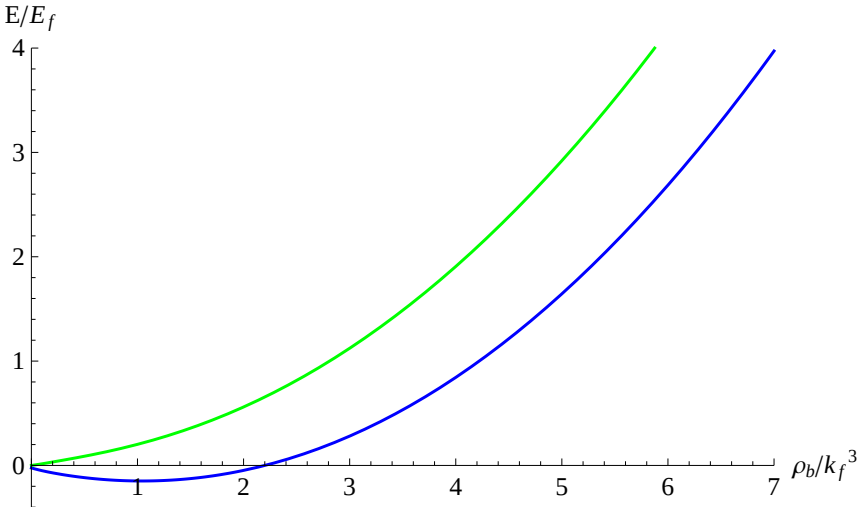

Figure 3.4: *plot of the free energy as a function of ρ_b showing the second-order phase transition for the Bose-Fermi mixture as we move around in the plane of local chemical potentials where the local minimum is continuous from $\rho_{min} = 0$ to $\rho_{min} \neq 0$. From the top to the bottom,each curve corresponds to different values of μ_b/E_f=-0.14 and μ_f/E_f= -0.9045 and 0.8954*

3.5 Zero-temperature quantum phase diagram

After we have characterized the phase transition in terms of its order, we are able to discuss the quantum phase diagram for the local resonant Bose-Fermi mixtures. To analyse the phase boundary, we fix $\tilde{V}$, $\tilde{V}_{bg}$ and $\tilde{g}$, and search for phase transitions in the plane $(\tilde{\mu}_f, \tilde{\mu}_b)$ for $\tilde{\nu} = 0$. However, the choice of $\tilde{\nu} = 0$ gives all the different types of phase transitions for the Bose-Fermi mixtures.

Figure 3.5 corresponds to the resonance $\tilde{\nu} = 0$ with the local chemical potentials of fermions and bosons in the range of $\tilde{\mu}_f \in (-1.0, 0.45)$ and $\tilde{\mu}_b \in (-0.26, 0.004)$. The chemical potentials $\mu_{b,f}$ are local such that $\mu_{b,f} \equiv \mu_{b,f}(\mathbf{R})$. An important aspect of Bose-Fermi mixtures in the trap concerns the discontinuity observed in the density profiles. This discontinuity results from the crossing between the Bose-Einstein condensate (BEC) and the normal phase (N) around the first-order boundary due to the phase separation. The main phase is constantly BEC with one Fermi surface (FS) in the upper band, as shown in the phase diagram. The lower band can be either N or BEC with varying numbers of FS.

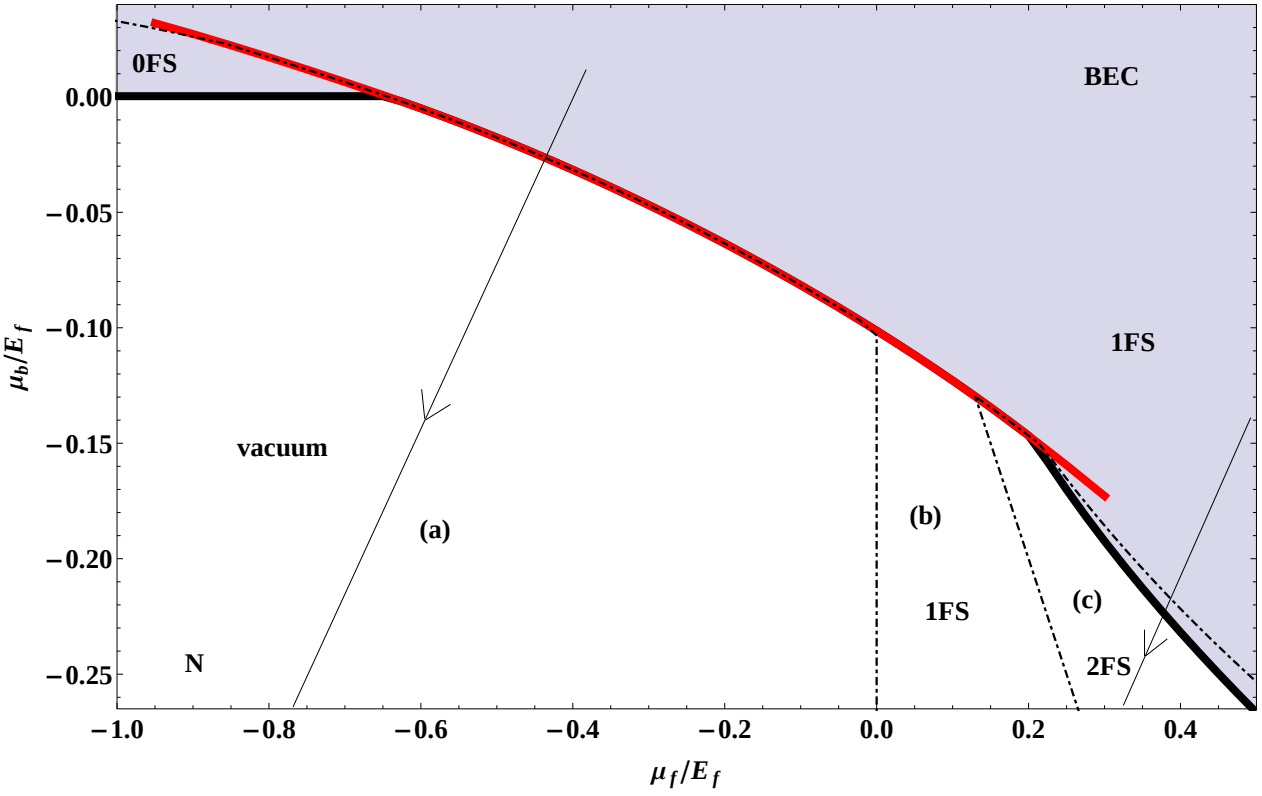

Figure 3.5: *Quantum phase diagram for zero detuning, $\nu = 0$ in the local chemical potential plane. The normal phase (white region) and the BEC- phase (gray region) determine the phase transition. The phase transition can be of first-order (red line) or second-order (black line). The dotted-dashed lines in the diagram separates regions with a different number of Fermi surfaces.*

By analysing the diagram, we see the red the first-order phase transition boundary, (red line lying on top of black line) and numerically it takes long to calculate. We obtain this line by the recursion method on the minimum of the energy that depends on. For a given value of $\tilde{\mu}_f$ we solve for different values of $\tilde{\mu}_b$ to get all possible values of $(\tilde{\mu}_f, \tilde{\mu}_b)$ where the density of bosons is discontinuous. As for the number Fermi surfaces, it is obtained with the recursive method for positive nonzero values $k_f^{\alpha,\beta}(\mathbf{R})$ roots of equation $\lambda_{\alpha,\beta}(k, \mathbf{R})$=0.

The black solid line marks the second-order phase transition boundary where the minimum is

continuous from the phase without BEC ($\rho_{min} = 0$) to the phase with BEC ($\rho_{min} \neq 0$). The boundaries obtained from the energy minimization divide the phase diagram in four regions. These regions are distinguished by the presence or absence of BEC, and the number of Fermi surfaces.

Hence, in region (a) we are in the vacuum state where the densities of particles ρ_b, ρ_f and ρ_m are equal to zero. The reason is that all states in the bands have positive energy. In this region the minimum of energy is zero for $\mu_f \leq 0$ and $\mu_f + \mu_b \leq \nu$. We have three sequences of phase transitions:

• The second-order phase transition from the vacuum to the BEC and the first-order phase transition from 0FS to 1FS for the hybrid fermion with energy $\lambda_\alpha(k, \mathbf{R})$ in which the value of ρ_{min} goes from zero to nonzero. It happens as we increase the chemical potential $\mu_b \geq 0$ from the top left of the phase diagram.

• The first-order phase transition BEC-BEC characterized by the jump in the value of ρ_{min} is seen before the end of the red line when μ_b is increasing further which push ρ_{min} to increase also. This will lower the value of the energy localized at the second minimum which is nonzero where the first-order phase transition arises.

• From the right we encounter the first-order phase transition from the normal phase to the BEC and second-order Fermi surface changing phase from 0FS to 1FS. We count the number of Fermi surface by changing the chemical potential. The lines where μ_f and $\mu_f + \mu_b = 0$ define the Fermi surface phase transition boundary.

The region (b), for which $\mu_f > 0$, we have a Fermi surface of hybrid fermions with energy $\lambda_\alpha(k, \mathbf{R})$, while for the hybrid fermions $\lambda_\beta(k, \mathbf{R})$ is empty because the dispersion relation $\lambda_\beta(k, \mathbf{R})$=0, in this region. We have the first-order phase transition with BEC as we cross the upper boundary (red line).

The lowest region (c) on the right shows the presence of two Fermi surfaces of atoms and molecules without a condensate. The absence of the condensate in the normal phase causes the energy of mixed fermions to increase for a large enough fermionic chemical potential. We encounter the second-order phase transition from zero condensate to a phase with a condensate. This phase is followed by the Fermi surfaces changing phase (2FS to 1FS). The transition line on the top (red line) is the first-order phase transition for the BEC and FS phases. The upper gray region corresponds to the condensation of mostly bosons favoured by induced attraction due to the cloud of hybrid fermions. We also have a FS transition of free fermions.

By using the law of number-conservation constraints, we state also locally that for every molecule arising from the binding between boson and fermion, there is one less free boson and fermion in the system as shown in Refs. [42]. It shows that the total number density of bosons or fermions is equal to the number density of bosons in the condensate or fermions including those contained in the molecules,

$$\rho_b^0(\mathbf{R}) = \rho_b(\mathbf{R}) + \rho_m(\mathbf{R}) \tag{3.5.1a}$$

$$\rho_f^0(\mathbf{R}) = \rho_f(\mathbf{R}) + \rho_m(\mathbf{R}). \tag{3.5.1b}$$

From these relations, we obtained the plot of density profiles of species corresponding to the

first-order phase transition as shown in Fig.3.6 and the second-order phase transition given in Fig.3.7 as we move around the chemical potential plane with the trajectories given by the arrows in Fig.3.5 .

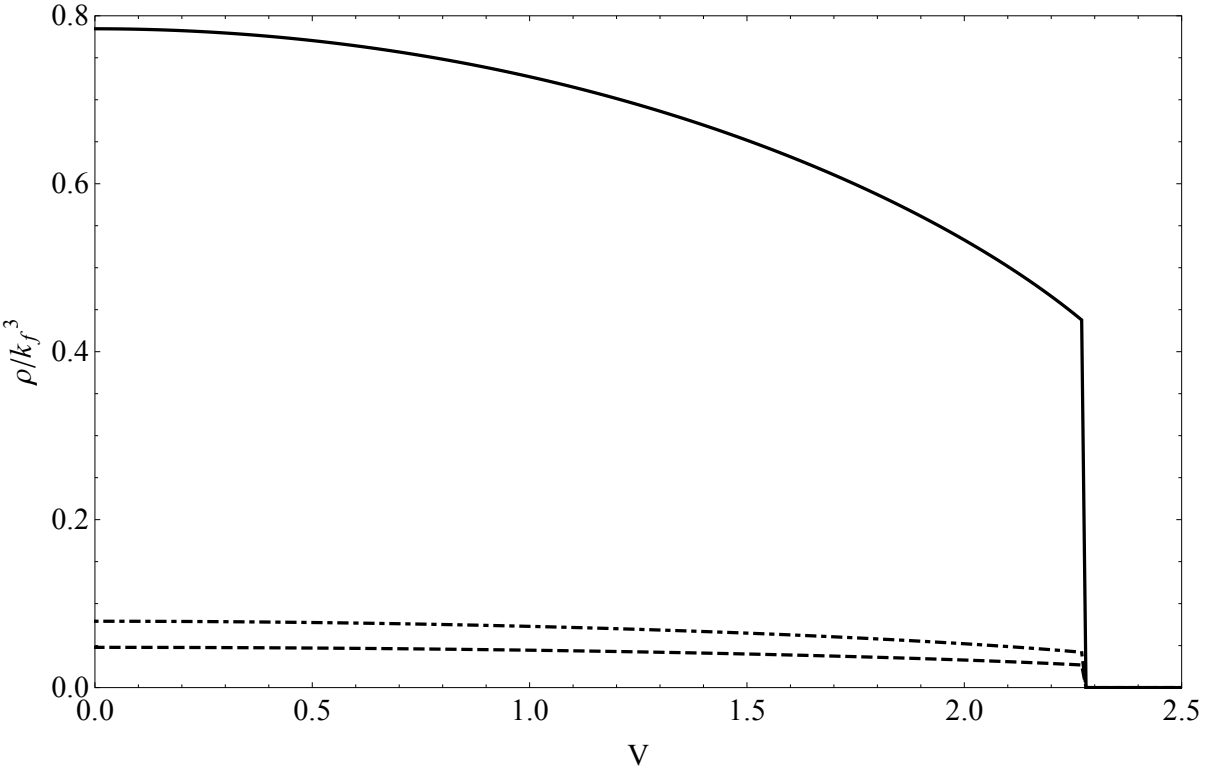

Figure 3.6: *Local density profiles of condensed bosons (solid lines), fermions (dashed lines) and molecules (dotted-dashed lines)as a function of V, which parametrises the lines in the phase diagram. We see the discontinuity predicted before as we move along the trajectory crossing the red line in the phase diagram.*

,

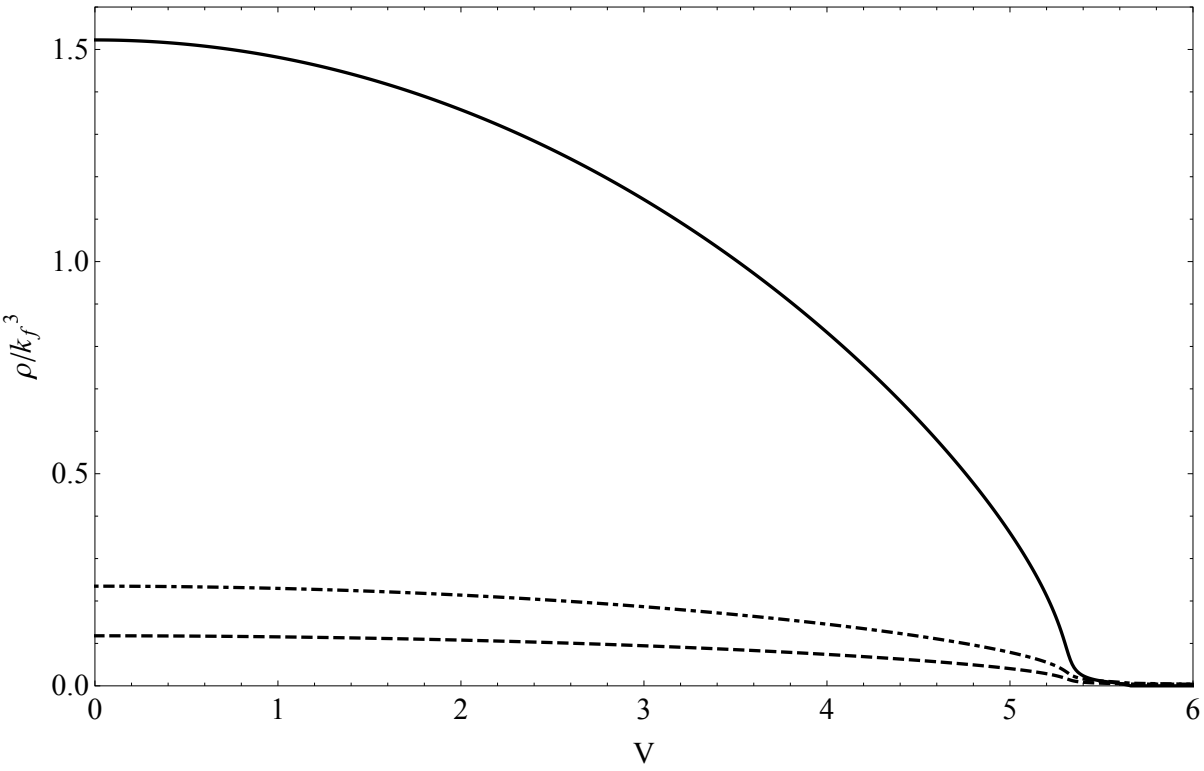

Figure 3.7: *Local density profile of condensed bosons (solid lines), fermions (dashed lines) and molecules (dotted-dashed lines) as a function of V, which parametrises the lines in the phase diagram. The continuity is shown as we move along the trajectory crossing the Black line in the phase diagram.*

3.6 Global properties of the system in the trap

The theory so far has been presented at any localised point in the space analogous to the homogeneous case. We would like to examine the global thermodynamic properties, and possibility of superfluidity signatures in the mixture for different values of the detuning and the trap aspect ratio of the harmonic oscillator. Since current experiments with ultracold atoms are carried out with fixed particle number, we consider N particles trapped by the external potential. We have to find the chemical potential values that fix the total number of particles of each specie in the mixture. The full quantum mechanical theory regarding the trapped Bose-Fermi system has already been stated in the previous sections with the use of a local density approximation. However, the effect of the trap comprise of writing the local chemical potentials, as stated earlier in Eq.(3.3.8), as

$$\mu_{b,f}(\mathbf{R}) = \mu^0_{b,f} - V^{b,f}_{trap}(\mathbf{R}). \tag{3.6.1}$$

Here we consider the Fermi energy to be greater than the level spacing of the harmonic oscillator. We will see right away that the geometry of the trap through the **R**-dependence of all quantities describing the system, such the densities, strongly modify the thermodynamics of the system for a given value of the detuning. In our calculations, we will vary ω_z by keeping $\omega_\perp$, fixed which will influence the results obtained from this model.

We note that the resonant mixtures are different from any other dilute non-resonant mixtures,

because of additional terms in the Hamiltonian. For a non-resonant mixture, the weak attraction between bosons and fermions is the only relevant interaction. It turns out that the bosons will occupy a single quantum state (ground state) to form a pure Bose-Einstein condensate (BEC), including a depletion due quantum fluctuations around the ground state. While the fermions on the other hand will fill a Fermi sphere of radius k_f. In this case the Hamiltonian reads[21]

$$\begin{aligned}\hat{H} = \int d\mathbf{x}d\mathbf{y}\Big[&\Psi_b^\dagger(\mathbf{x})T_b(\mathbf{x},\mathbf{y})\Psi_b(\mathbf{y}) + \Psi_f^\dagger(\mathbf{x})T_f(\mathbf{x},\mathbf{y})\Psi_f(\mathbf{y}) \\ &+ \frac{1}{2}\int d\mathbf{x}'d\mathbf{y}'\Psi_b^\dagger(\mathbf{x})\Psi_b^\dagger(\mathbf{y})V(\mathbf{x},\mathbf{y},\mathbf{x}',\mathbf{y}')\Psi_b(\mathbf{y}')\Psi_b(\mathbf{x}') \quad . \\ &+ \int d\mathbf{x}'d\mathbf{y}'\Psi_b^\dagger(\mathbf{x})\Psi_f^\dagger(\mathbf{y})V_{bg}(\mathbf{x},\mathbf{y},\mathbf{x}',\mathbf{y}')\Psi_f(\mathbf{y}')\Psi_b(\mathbf{x}')\Big]\end{aligned} \tag{3.6.2}$$

Effectively, when the attraction between the two distinct species is modified around Feshbach resonances, a bound state made of one boson and one fermion is formed. The new Hamiltonian, as suggested in Eq.(3.1.1), contains the molecular field $\Psi_m(\mathbf{x})$, introduced intuitively to take into account the Feshbach resonances, and the coupling interaction $g(\mathbf{x},\mathbf{y})$ that acts as a perturbative term.

We then need a self-consistent method to solve the Eqs.(3.3.17), (3.3.18), (3.3.19) and (3.4.2). We choose the coupling constant g to be very small, since we are working in the resonant regime which possible formation of molecules. We have the following steps that allow us to solve the problem:

• From the Eq.(3.4.2), we find the root, ρ_{min}, corresponding to the minimum of energy for given values of $\mu_b(\mathbf{R})$ and $\mu_f(\mathbf{R})$ obtained from the local chemical potentials in Eq(3.6.1). These values of the root and chemical potentials are used to find the densities $\rho_{f,m}(\mathbf{R})$.

• At each step, the chemical potentials of the Bose gas and Fermi gas are modified until the normalization conditions $\int d^3\mathbf{R}(\rho_b(\mathbf{R}) + \rho_m(\mathbf{R})) = N_B^0$ and $\int d^3\mathbf{R}(\rho_f(\mathbf{R}) + \rho_m(\mathbf{R})) = N_f^0$ yield the desired number of particles.

• The observable quantities such as density $\rho_{b,f,m}(\mathbf{R})$ can now be evaluated using the resulting values of $\mu_{b,f}$ that fix the number of atoms in the system.

The illustrations of Fig.3.8 and Fig.3.9 report the radial densities when we are moving along the z-axis of bosons, fermions and molecules obtained after integration of Eqs.(3.3.17), (3.3.18), (3.3.19), and (3.4.2) for $\lambda = 0.01$ and 0.5 when the number of bosons exceeds the number of fermions ($N_b > N_f$). This is done for different values of the detuning ν, because the interaction near Feshbach resonances depends on the detuning ν. The signature of a superfluidity phase, predicted before, appears in the bulge of the density in the center of the trap. As in most experiments, all condensed bosons accumulate in the center of the trap where their density is much larger than that of fermions. This is due to Pauli blocking that keep fermions away as their density spread out from the center of the trap, and the interaction between bosons and fermions. For the two different values of λ, the distributions in both figures are markedly different in the centre of the trap, but have a common behaviour. Particularly, we see that by increasing the trap aspect ratio, λ, there is a change in the shape of the trapping potential. This change causes the peaks of the densities to decrease in the center of the trap, which increase the extent of the densities along the radial axis.

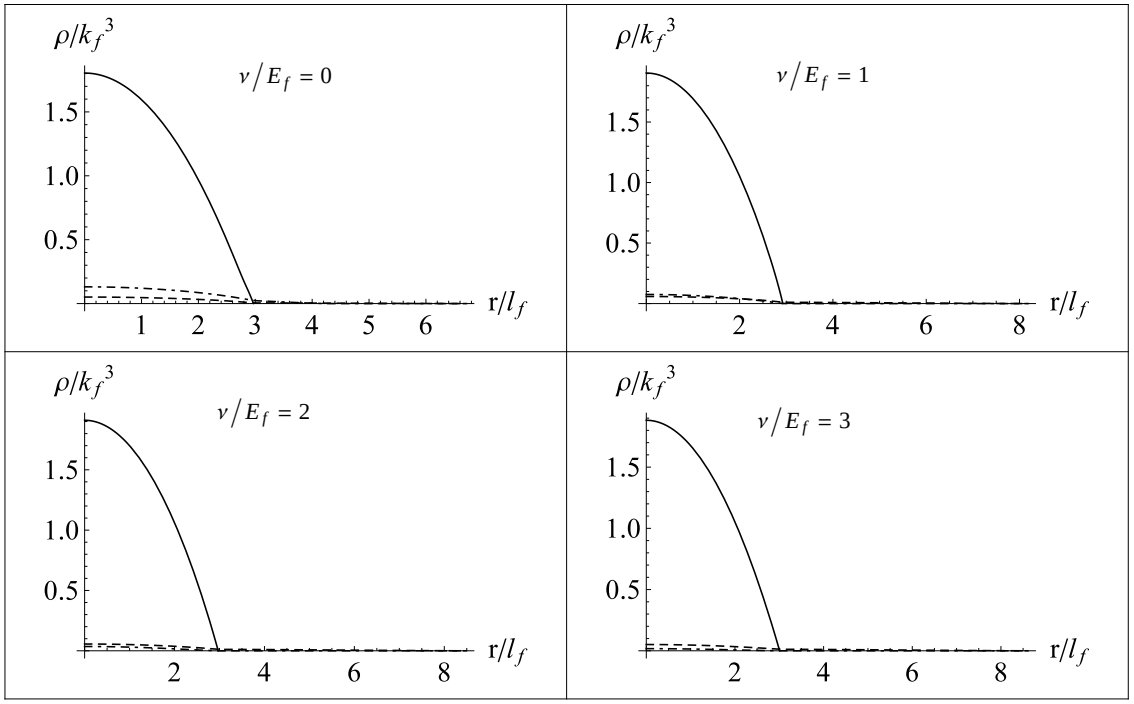

Figure 3.8: *Density profiles for $\lambda = 0.01$ in the harmonic trap as a function of $r = \lambda z$ of condensed boson number (solid lines), fermion number (dashed lines) and molecule number (dashed-dotted lines) for different values of the detuning $\nu/E_f = 0, 1, 2, 3$. We note the peak in the center of the trap showing the accumulation of particles for $N_b > N_f$.*

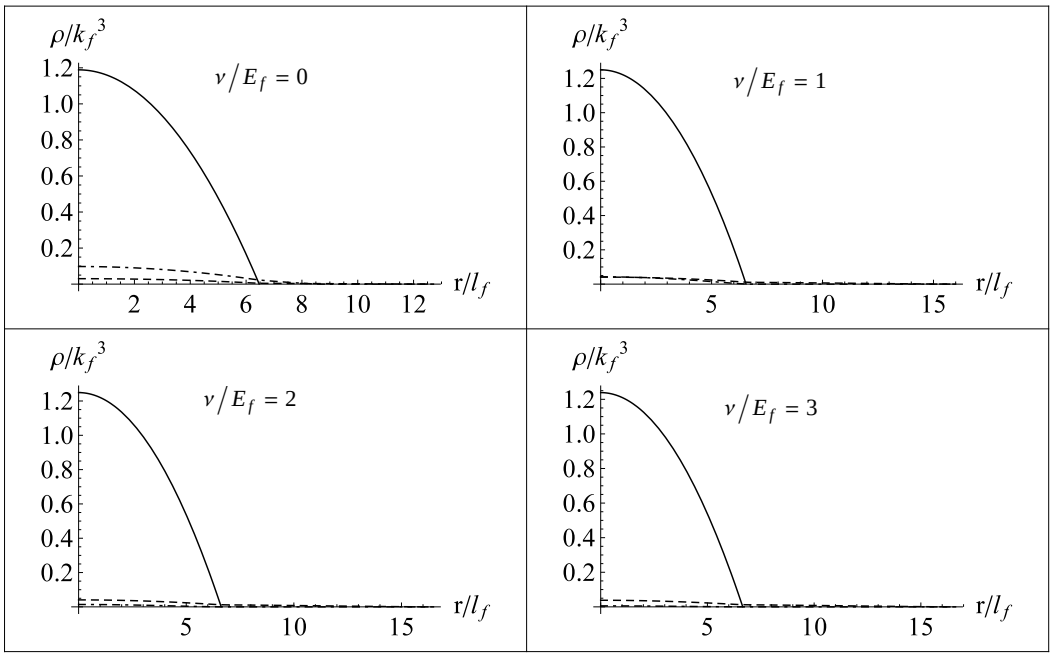

Figure 3.9: *Density profiles for $\lambda = 0.5$ in the harmonic trap as a function $r = \lambda z$ of condensed boson number (solid lines), fermion number (dashed lines) and molecule number (dashed-dotted lines) for different values of the detuning $\nu/E_f = 0, 1, 2, 3$. We note the peak in the center of the trap showing the accumulation of particles for $N_b > N_f$.*

Analysing the two figures, we start with $\nu = 0$, the regime where molecule formation is favourable. We see the coalescence of a condensate, Fermi surfaces of atoms and molecules in the gas with their peaks in the center of the trap. For $\nu > 0$ we move in the energetically unfavourable regime. The molecule population starts to decrease and disappears for sufficiently large detuning, to decay into a pair of atoms made of one boson and one fermion. The pair of atoms can meet again to create a molecule for detuning close to resonance. From our numerical results, this happens when $\nu > \mu_b + \mu_f$. Hence for large detuning, it will remain the only Fermi surface of atoms in the system and free bosons. There is not much change in the boson and fermion atomic densities afterwards, because bosons released after the molecules have decayed will remain unpaired and will not condense. This will give rise to an unconventional Bose liquid, while the fraction of unpaired fermions will lead to conventional Fermi liquid, as described in Ref. [37], for the fermionic atom number exceeding that of bosons. The plot in Fig.3.10 shows the corresponding total number of bosons, fermions and molecules as a function of the detuning ν. Therefore, for the negative values of ν, the population of molecules and bosons are stable while fermions are almost non-existent, since these have all been turned into molecules. The number of molecules start decreasing as we draw near $\nu = 0$, and disappear for large enough detuning. This causes the number of bosons and fermions to increase and stabilize because all molecules have decayed to release bosons and fermions. These results agree with those obtained by Bartolotti et al.[42].

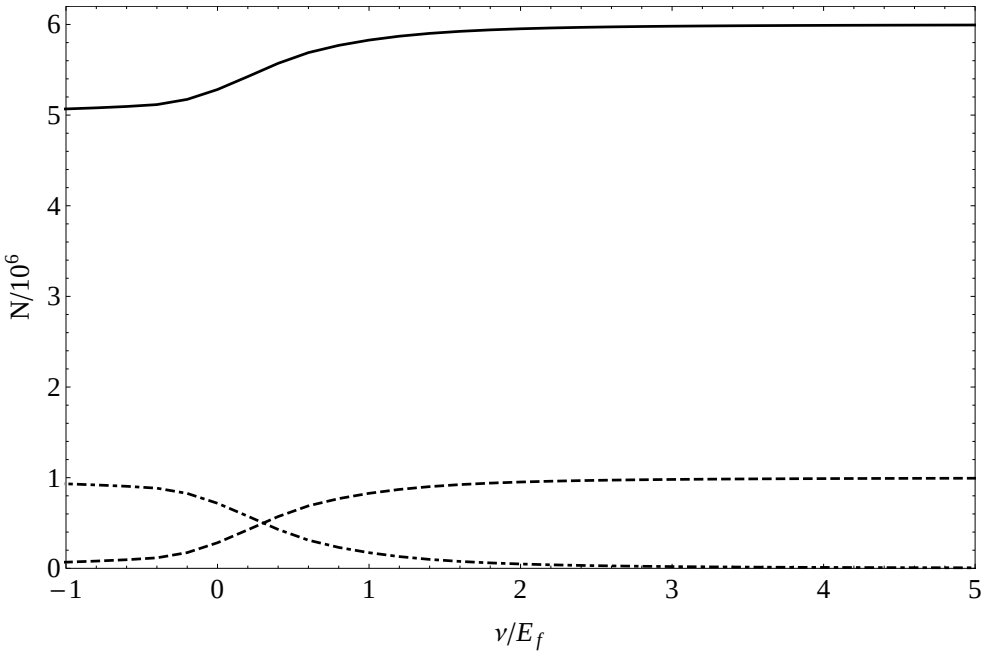

Figure 3.10: *Population of condensed bosons (solid lines), fermions (dashed lines) and molecules (dashed-dotted lines) as a function of the detuning ν/E_f for $N_b > N_f$.*

In contrast, the case where the fermions outnumber the bosons is shown in Fig.3.11 and Fig.3.12 for $\lambda = 0.01$ and 0.5, and for different values of the detuning. No bosons are present at $\nu = 0$, since there are enough fermions to turn all bosonic atoms into molecules. We only have two Fermi

surfaces in the gas, one made of atoms and another of molecules. As we increase the detuning, we see the appearance of released bosons which cluster in the center of the trap by forming a pure Bose-Einstein condensate. This causes the number of molecules to decrease and disappear for large detuning and leaving one Fermi surface of atoms. The peak of fermions in the center of the trap decreases and stays stable due to the presence of the condensate in the system. There is also the presence of unpaired bosons and fermions in the gas.

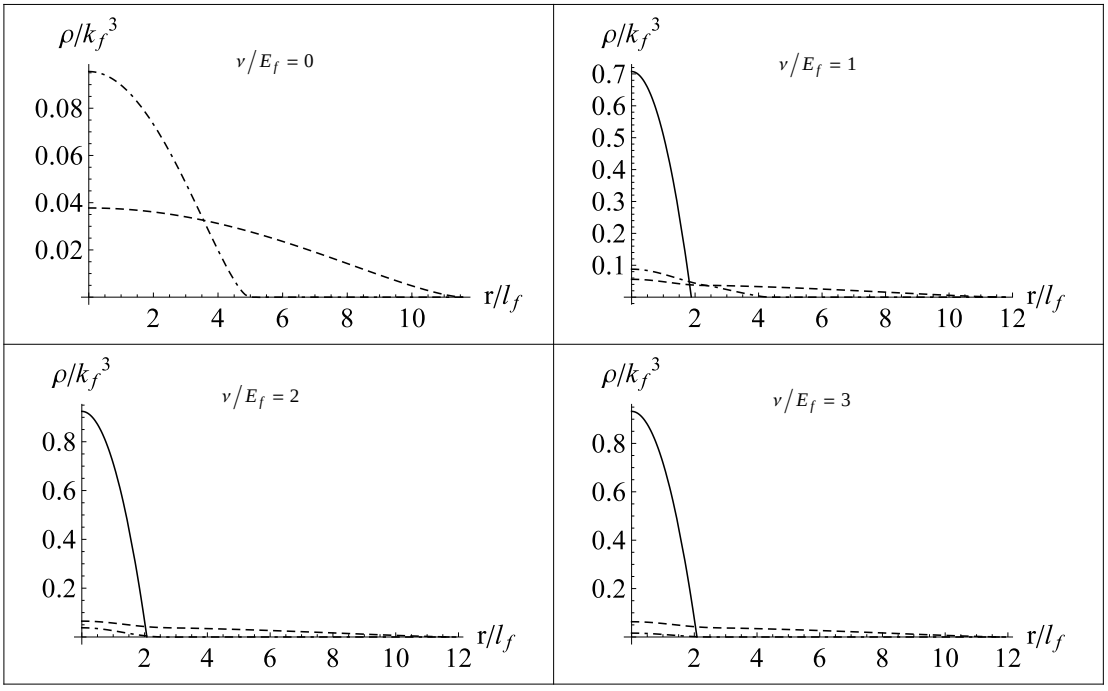

Figure 3.11: *Density profiles for $\lambda = 0.01$ in the harmonic trap as a function $r = \lambda z$ of condensed boson number (solid lines), fermion number (dashed lines) and molecule number (dashed-dotted lines) for different values of the detuning $\nu/E_f = 0, 1, 2, 3$. We note the peak in the center of the trap showing the accumulation of particles for $N_b < N_f$.*

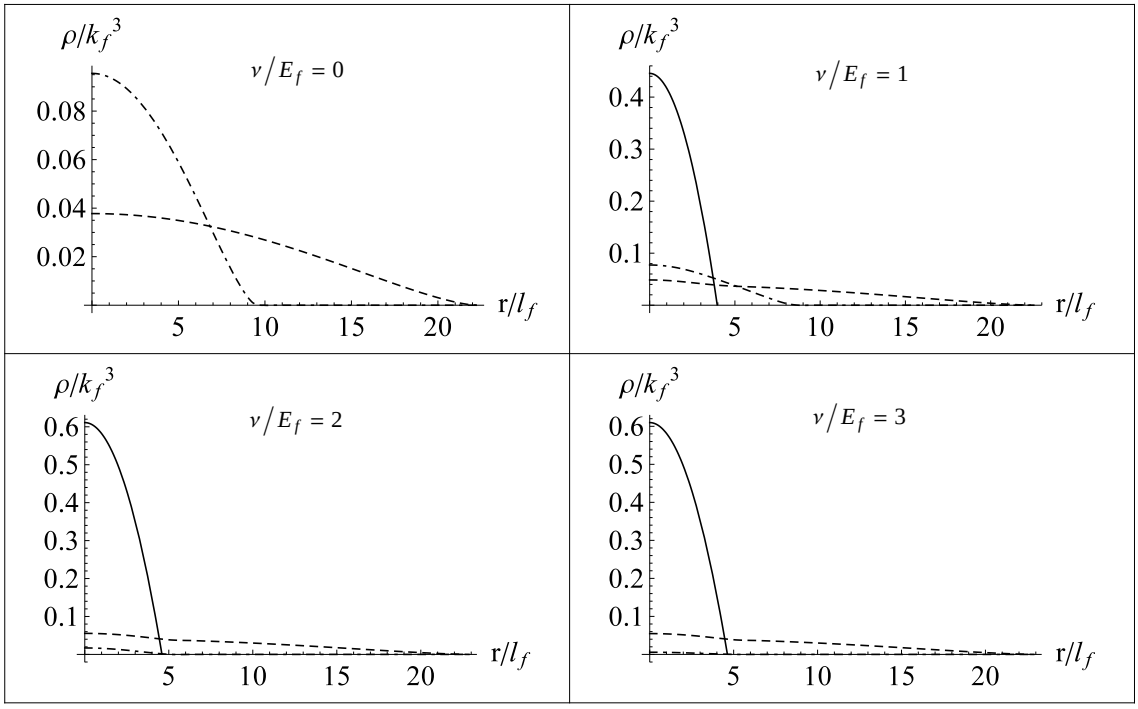

Figure 3.12: *Densities profile for $\lambda = 0.5$ in the harmonic trap as a function of $r = \lambda z$ of condensed boson number (solid lines), fermion number (dashed lines) and molecule number (dashed-dotted lines) for different values of the detuning $\nu/E_f = 0, 1, 2, 3$. We note the peak in the center of the trap showing the accumulation of particles for $N_b < N_f$.*

The plot in Fig.3.13 gives the population of the total number of species in the system. We see clearly that no bosons are present for negative detuning. For $\nu > 0$ we see a growth in their number as the molecule population starts decaying. This causes the population of fermions, initially stable, to grow and stabilise until all molecules in the system have decayed.

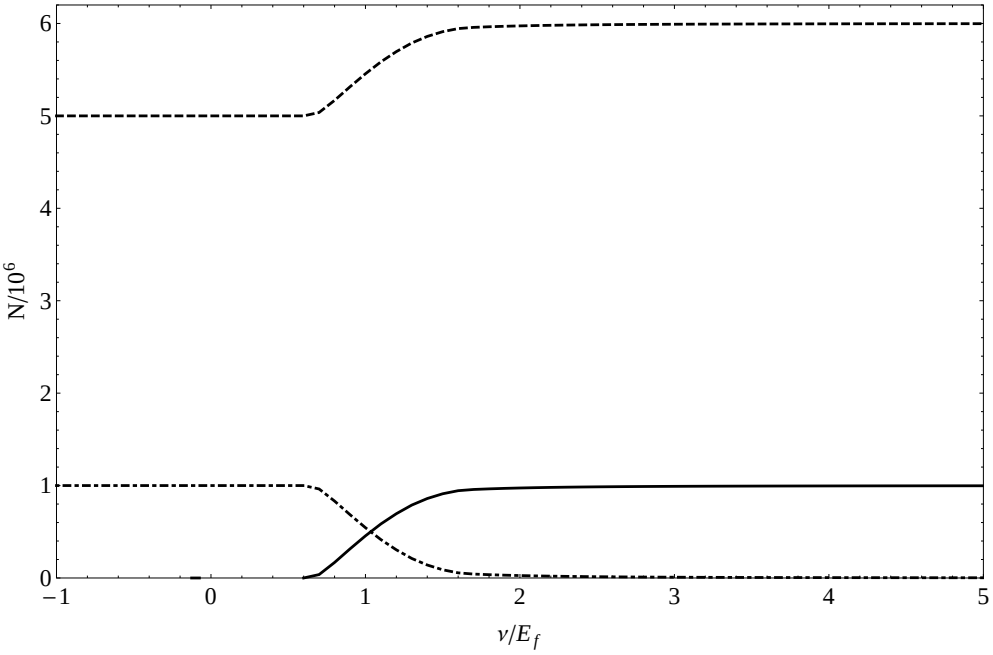

Figure 3.13: *Population of condensed bosons (solid lines), fermions (dashed lines) and molecules (dashed-dotted lines) as a function of the detuning ν/E_f for $N_b < N_f$.*

3.7 Summary of results

In this chapter we have investigated the physics of resonant Bose-Fermi mixtures confined to a harmonic potential near a narrow Feshbach resonance. We have analysed the static properties of the mixtures by first describing the basic structure of the quantum phase diagram using the mean-field theory. The local density approximation provides a good way to alleviate difficulties due to the presence of the trapping potential. Since this breaks down the symmetry of the problem, we assumed a slow varying on the trapping potential. The system has been treated locally to recover all the results as in the case of a homogeneous system. We saw that the many-body ground state energy can be expressed in terms of densities of both species and the detuning, which is the binding energy of the molecules. We have found that mixtures at zero detuning, $\nu = 0$, exhibit a variety of phases containing both normal (non-BEC) and BEC phase, including the number of Fermi surfaces resulting from the hybridization among fermionic atoms and molecules. Moreover, we have analysed the local density distribution of particles in terms of the parameter V related to the trapping potential for the first-order and second-order phase transitions. Finally, we addressed the global properties of the entire system for a fixed number of particles in the trap for different values of the detuning ν and the trap aspect ratio λ. We have examined several cases that favour the formation of molecules when the number of bosons is either greater or less than the number of the fermions. We have seen that the geometry of the trap, which depends on the trap aspect ratio, λ, affects the density of species. We also noticed that the boson-fermion interaction suppresses the fermionic density in the center of the trap where the density of the condensate peaks at different regimes related to the detuning ν when the number of fermions is greater than the number of bosons.

Chapter 4

Conclusions and outlook

In this thesis we have presented an analysis of a trapped Bose-Fermi mixture with an interaction controlled by a Feshbach resonance. We began by considering the scattering of neutral atoms in the low energy limit. We saw that two types of resonances can play a role in the scattering process of neutral atoms: the shape or potential resonance and the Feshbach resonance. The first is a single channel resonance occurring when quasi-bound states are created in the continuum by the potential barrier. These bound states are shadows of real bound states and eventually decay into free states. There are experimental limitations in modifying the interaction with these types of resonances. In contrast, Feshbach resonances have a multichannel nature and occur when the energy of the colliding atoms in the open channels matches the energy of a true bound state in the closed channel. If there is coupling between the channels transitions might occur during the scattering where quantum features of the system can be explored. We have focused on two-channel resonances induced by an external magnetic field which allows for the tuning of interactions between particles. This is due to the internal structure of atoms and make Feshbach resonance experiments powerful tools for investigating quantum many-body effects.

Our treatment of trapped Bose-Fermi mixtures was based on the mean-field and local density approximations. analysing these models with the aid of computational methods allowed us to fully explore the system's rich phase structure. We observed phase transitions associated with continuous and discontinuous changes in the boson condensate density, as well as changes in the number of quasi-particle Fermi surfaces. The latter is also closely related to the formation of molecules. We also considered the case of a closed system with a fixed total number of particles. Here we investigated the effect of the detuning and trap profile on the particle numbers and density profiles of the various species. We found that our results were in very good agreement with those in the literature [37, 40, 42, 72].

There are undeniable limitations to the approach we have followed here. While the mean-field approximation allows the Hamiltonian to be brought into a solvable quadratic form, it has significant shortcomings. In particular, it does not correctly account for the depletion of the condensate

due to quantum fluctuations or the three-body correlations which describe the coupling of the molecules to non-condensed bosons.

Despite its shortcomings this study has provided useful insight into the qualitative phase structure of resonant Bose-Fermi mixtures. Furthermore, related studies suggest that our formalism can be adapted straightforwardly to study trapped mixtures away from equilibrium [85] or at finite temperatures.

List of References

[1] C. C. Bradley, C. A. Sackett, J. J. Tollett, and R. G. Hulet. Evidence of bose-einstein condensation in an atomic gas with attractive interactions. *Phys. Rev. Lett.*, 75:1687–1690, Aug 1995.

[2] K. B. Davis, M. O. Mewes, M. R. Andrews, N. J. van Druten, D. S. Durfee, D. M. Kurn, and W. Ketterle. Bose-einstein condensation in a gas of sodium atoms. *Phys. Rev. Lett.*, 75:3969–3973, Nov 1995.

[3] G. Roati, F. Riboli, G. Modugno, and M. Inguscio. Fermi-bose quantum degenerate ^{40}K-^{87}Rb mixture with attractive interaction. *Phys. Rev. Lett.*, 89:150403, Sep 2002.

[4] Z. Hadzibabic, C. A. Stan, K. Dieckmann, S. Gupta, M. W. Zwierlein, A. Görlitz, and W. Ketterle. Two-species mixture of quantum degenerate bose and fermi gases. *Phys. Rev. Lett.*, 88:160401, Apr 2002.

[5] C. A. Stan, M. W. Zwierlein, C. H. Schunck, S. M. F. Raupach, and W. Ketterle. Observation of feshbach resonances between two different atomic species. *Phys. Rev. Lett.*, 93:143001, Sep 2004.

[6] Nicolai Nygaard and Klaus Mølmer. Component separation in harmonically trapped boson-fermion mixtures. *Phys. Rev. A*, 59:2974–2981, Apr 1999.

[7] R. Roth and H. Feldmeier. Mean-field instability of trapped dilute boson-fermion mixtures. *Phys. Rev. A*, 65:021603, Jan 2002.

[8] Robert Roth. Structure and stability of trapped atomic boson-fermion mixtures. *Phys. Rev. A*, 66:013614, Jul 2002.

[9] Hui Hu and Xia-Ji Liu. Thermodynamics of a trapped bose-fermi mixture. *Phys. Rev. A*, 68:023608, Aug 2003.

[10] Hui Hu and Xia-Ji Liu. Thermodynamics of a trapped bose-fermi mixture. *Phys. Rev. A*, 68:023608, Aug 2003.

[11] Xia-Ji Liu, Michele Modugno, and Hui Hu. Finite-temperature effects on the collapse of trapped bose-fermi mixtures. *Phys. Rev. A*, 68:053605, Nov 2003.

[12] Sadhan K. Adhikari. Mean-field description of a dynamical collapse of a fermionic condensate in a trapped boson-fermion mixture. *Phys. Rev. A*, 70:043617, Oct 2004.

[13] Sadhan K. Adhikari. Fermionic bright soliton in a boson-fermion mixture. *Phys. Rev. A*, 72:053608, Nov 2005.

[14] Rina Kanamoto and Makoto Tsubota. Phase separation of a fast rotating boson-fermion mixture in the lowest-landau-level regime. *Phys. Rev. Lett.*, 96:200405, May 2006.

[15] Takayuki Watanabe, Toru Suzuki, and Peter Schuck. Bose-fermi pair correlations in attractively interacting bose-fermi atomic mixtures. *Phys. Rev. A*, 78:033601, Sep 2008.

[16] M. J. Bijlsma, B. A. Heringa, and H. T. C. Stoof. Phonon exchange in dilute fermi-bose mixtures: Tailoring the fermi-fermi interaction. *Phys. Rev. A*, 61:053601, Apr 2000.

[17] H. Heiselberg, C. J. Pethick, H. Smith, and L. Viverit. Influence of induced interactions on the superfluid transition in dilute fermi gases. *Phys. Rev. Lett.*, 85:2418–2421, Sep 2000.

[18] D. V. Efremov and L. Viverit. p-wave cooper pairing of fermions in mixtures of dilute fermi and bose gases. *Phys. Rev. B*, 65:134519, Mar 2002.

[19] L. Viverit. Boson-induced s-wave pairing in dilute boson-fermion mixtures. *Phys. Rev. A*, 66:023605, Aug 2002.

[20] F. Matera. Fermion pairing in bose-fermi mixtures. *Phys. Rev. A*, 68:043624, Oct 2003.

[21] A. P. Albus, S. A. Gardiner, F. Illuminati, and M. Wilkens. Quantum field theory of dilute homogeneous bose-fermi mixtures at zero temperature: General formalism and beyond mean-field corrections. *Phys. Rev. A*, 65:053607, Apr 2002.

[22] M. Lewenstein, L. Santos, M. A. Baranov, and H. Fehrmann. Atomic bose-fermi mixtures in an optical lattice. *Phys. Rev. Lett.*, 92:050401, Feb 2004.

[23] A. Sanpera, A. Kantian, L. Sanchez-Palencia, J. Zakrzewski, and M. Lewenstein. Atomic fermi-bose mixtures in inhomogeneous and random lattices: From fermi glass to quantum spin glass and quantum percolation. *Phys. Rev. Lett.*, 93:040401, Jul 2004.

[24] Alexander Albus, Fabrizio Illuminati, and Jens Eisert. Mixtures of bosonic and fermionic atoms in optical lattices. *Phys. Rev. A*, 68:023606, Aug 2003.

[25] H. P. Büchler and G. Blatter. Phase separation of atomic bose-fermi mixtures in an optical lattice. *Phys. Rev. A*, 69:063603, Jun 2004.

[26] Kenneth Günter, Thilo Stöferle, Henning Moritz, Michael Köhl, and Tilman Esslinger. Bose-fermi mixtures in a three-dimensional optical lattice. *Phys. Rev. Lett.*, 96:180402, May 2006.

[27] Robert Roth and Keith Burnett. Quantum phases of atomic boson-fermion mixtures in optical lattices. *Phys. Rev. A*, 69:021601, Feb 2004.

[28] I. Titvinidze, M. Snoek, and W. Hofstetter. Supersolid bose-fermi mixtures in optical lattices. *Phys. Rev. Lett.*, 100:100401, Mar 2008.

[29] M. W. J. Romans, R. A. Duine, Subir Sachdev, and H. T. C. Stoof. Quantum phase transition in an atomic bose gas with a feshbach resonance. *Phys. Rev. Lett.*, 93:020405, Jul 2004.

[30] Leo Radzihovsky, Jae Park, and Peter B. Weichman. Superfluid transitions in bosonic atom-molecule mixtures near a feshbach resonance. *Phys. Rev. Lett.*, 92:160402, Apr 2004.

[31] S. J. J. M. F. Kokkelmans, J. N. Milstein, M. L. Chiofalo, R. Walser, and M. J. Holland. Resonance superfluidity: Renormalization of resonance scattering theory. *Phys. Rev. A*, 65:053617, May 2002.

[32] Y. Ohashi and A. Griffin. Bcs-bec crossover in a gas of fermi atoms with a feshbach resonance. *Phys. Rev. Lett.*, 89:130402, Sep 2002.

[33] Y. Ohashi and A. Griffin. Superfluid transition temperature in a trapped gas of fermi atoms with a feshbach resonance. *Phys. Rev. A*, 67:033603, Mar 2003.

[34] Alexander V Avdeenkov. Heat capacity of a two-component superfluid fermi gas. *Journal of Physics B: Atomic, Molecular and Optical Physics*, 37(1):237, 2004.

[35] C. A. Regal, M. Greiner, and D. S. Jin. Observation of resonance condensation of fermionic atom pairs. *Phys. Rev. Lett.*, 92:040403, Jan 2004.

[36] Daw-Wei Wang. Strong-coupling theory for the superfluidity of bose-fermi mixtures. *Phys. Rev. Lett.*, 96:140404, Apr 2006.

[37] Elisa Fratini and Pierbiagio Pieri. Pairing and condensation in a resonant bose-fermi mixture. *Phys. Rev. A*, 81:051605, May 2010.

[38] Jun Liang Song, Mohammad S. Mashayekhi, and Fei Zhou. Fermi-bose mixtures near broad interspecies feshbach resonances. *Phys. Rev. Lett.*, 105:195301, Nov 2010.

[39] J. Dukelsky, C. Esebbag, P. Schuck, and T. Suzuki. Comment on "fermi-bose mixtures near broad interspecies feshbach resonances". *Phys. Rev. Lett.*, 106:129601, Mar 2011.

[40] D. Ludwig, S. Floerchinger, S. Moroz, and C. Wetterich. Quantum phase transition in bose-fermi mixtures. *Phys. Rev. A*, 84:033629, Sep 2011.

[41] Alexander V. Avdeenkov, Daniele C. E. Bortolotti, and John L. Bohn. Stability of fermionic feshbach molecules in a bose-fermi mixture. *Phys. Rev. A*, 74:012709, Jul 2006.

[42] D. C. E. Bortolotti, A. V. Avdeenkov, and J. L. Bohn. Generalized mean-field approach to a resonant bose-fermi mixture. *Phys. Rev. A*, 78:063612, Dec 2008.

[43] M. Zaccanti, C. D'Errico, F. Ferlaino, G. Roati, M. Inguscio, and G. Modugno. Control of the interaction in a fermi-bose mixture. *Phys. Rev. A*, 74:041605, Oct 2006.

[44] J. J. Zirbel, K.-K. Ni, S. Ospelkaus, J. P. D'Incao, C. E. Wieman, J. Ye, and D. S. Jin. Collisional stability of fermionic feshbach molecules. *Phys. Rev. Lett.*, 100:143201, Apr 2008.

[45] J.J. Sakurai and S.F. Tuan. *Modern Quantum Mechanics*. Addison-Wesley Publishing Company, 1994.

[46] R.L. Liboff. *Introductory Quantum Mechanics*. Addison-Wesley, 1992.

[47] L.E. Ballentine. *Quantum Mechanics: A Modern Development*. World Scientific, 2000.

[48] R.A. Duine and H.T.C. Stoof. Atom-molecule coherence in bose gases. *Physics Reports*, 396:115 – 195, 2004.

[49] C.J. Joachain. *Quantum collision theory*. North-Holland publishing company, Amsterdam, 1975.

[50] Herman Feshbach. A Unified theory of nuclear reactions. 2. *Annals Phys.*, 19:287–313, 1962.

[51] E. Tiesinga, A. J. Moerdijk, B. J. Verhaar, and H. T. C. Stoof. Conditions for bose-einstein condensation in magnetically trapped atomic cesium. *Phys. Rev. A*, 46:R1167–R1170, Aug 1992.

[52] E. Tiesinga, B. J. Verhaar, and H. T. C. Stoof. Threshold and resonance phenomena in ultracold ground-state collisions. *Phys. Rev. A*, 47:4114–4122, May 1993.

[53] Ph. Courteille, R. S. Freeland, D. J. Heinzen, F. A. van Abeelen, and B. J. Verhaar. Observation of a feshbach resonance in cold atom scattering. *Phys. Rev. Lett.*, 81:69–72, Jul 1998.

[54] J. L. Roberts, N. R. Claussen, James P. Burke, Chris H. Greene, E. A. Cornell, and C. E. Wieman. Resonant magnetic field control of elastic scattering in cold ^{85}rb. *Phys. Rev. Lett.*, 81:5109–5112, Dec 1998.

[55] A. Marte, T. Volz, J. Schuster, S. Dürr, G. Rempe, E. G. M. van Kempen, and B. J. Verhaar. Feshbach resonances in rubidium 87: Precision measurement and analysis. *Phys. Rev. Lett.*, 89:283202, Dec 2002.

[56] Vladan Vuletić, Andrew J. Kerman, Cheng Chin, and Steven Chu. Observation of low-field feshbach resonances in collisions of cesium atoms. *Phys. Rev. Lett.*, 82:1406–1409, Feb 1999.

[57] T. Bourdel, J. Cubizolles, L. Khaykovich, K. M. F̃. Magalhães, S. J. J. M. F̃. Kokkelmans, G. Ṽ. Shlyapnikov, and C. Salomon. Measurement of the interaction energy near a feshbach resonance in a ^{6}Li fermi gas. *Phys. Rev. Lett.*, 91:020402, Jul 2003.

[58] K. M. O'Hara, S. L. Hemmer, S. R. Granade, M. E. Gehm, J. E. Thomas, V. Venturi, E. Tiesinga, and C. J. Williams. Measurement of the zero crossing in a feshbach resonance of fermionic ^{6}Li. *Phys. Rev. A*, 66:041401, Oct 2002.

[59] K. Dieckmann, C. A. Stan, S. Gupta, Z. Hadzibabic, C. H. Schunck, and W. Ketterle. Decay of an ultracold fermionic lithium gas near a feshbach resonance. *Phys. Rev. Lett.*, 89:203201, Oct 2002.

[60] C. A. Regal and D. S. Jin. Measurement of positive and negative scattering lengths in a fermi gas of atoms. *Phys. Rev. Lett.*, 90:230404, Jun 2003.

[61] A. Simoni, F. Ferlaino, G. Roati, G. Modugno, and M. Inguscio. Magnetic control of the interaction in ultracold k-rb mixtures. *Phys. Rev. Lett.*, 90:163202, Apr 2003.

[62] C. A. Stan, M. W. Zwierlein, C. H. Schunck, S. M. F. Raupach, and W. Ketterle. Observation of feshbach resonances between two different atomic species. *Phys. Rev. Lett.*, 93:143001, Sep 2004.

[63] William C. Stwalley. Stability of spin-aligned hydrogen at low temperatures and high magnetic fields: New field-dependent scattering resonances and predissociations. *Phys. Rev. Lett.*, 37:1628–1631, Dec 1976.

[64] C. Ticknor, C. A. Regal, D. S. Jin, and J. L. Bohn. Multiplet structure of feshbach resonances in nonzero partial waves. *Phys. Rev. A*, 69:042712, Apr 2004.

[65] T. G. Tiecke, M. R. Goosen, J. T. M. Walraven, and S. J. J. M. F. Kokkelmans. Asymptotic-bound-state model for feshbach resonances. *Phys. Rev. A*, 82:042712, Oct 2010.

[66] Daniele Carlo Enrico Bortolotti. *Feshbach Resonances in Ultracold Bose-Fermi Mixtures*. PhD thesis, University of Colorado, 2007.

[67] A. J. Moerdijk, B. J. Verhaar, and A. Axelsson. Resonances in ultracold collisions of ^{6}Li, ^{7}Li, and ^{23}Na. *Phys. Rev. A*, 51:4852–4861, Jun 1995.

[68] V. Gurarie and L. Radzihovsky. Resonantly paired fermionic superfluids. *Annals of Physics*, 322:2 – 119, 2007.

[69] J.T.M. Walraven. Elements of quantum gases. 2010.

[70] Cheng Chin. A simple model of feshbach molecules. *cond-matter*, 0506313:1–5, 2005.

[71] Cheng Chin, Rudolf Grimm, Paul Julienne, and Eite Tiesinga. Feshbach resonances in ultracold gases. *Rev. Mod. Phys.*, 82:1225–1286, Apr 2010.

[72] Francesca M. Marchetti, Charles J. M. Mathy, David A. Huse, and Meera M. Parish. Phase separation and collapse in bose-fermi mixtures with a feshbach resonance. *Phys. Rev. B*, 78:134517, Oct 2008.

[73] Klaus Mølmer. Bose condensates and fermi gases at zero temperature. *Phys. Rev. Lett.*, 80:1804–1807, Mar 1998.

[74] L. Viverit, C. J. Pethick, and H. Smith. Zero-temperature phase diagram of binary boson-fermion mixtures. *Phys. Rev. A*, 61:053605, Apr 2000.

[75] Stephen Powell, Subir Sachdev, and Hans Peter Büchler. Depletion of the bose-einstein condensate in bose-fermi mixtures. *Phys. Rev. B*, 72:024534, Jul 2005.

[76] Francesca Ferlaino, Chiara D'Errico, Giacomo Roati, Matteo Zaccanti, Massimo Inguscio, Giovanni Modugno, and Andrea Simoni. Feshbach spectroscopy of a K-Rb atomic mixture. *Phys. Rev. A*, 73:040702, Apr 2006.

[77] N.N. Bogoliubov. On the theory of superfluidity. *J.Phys. (Moscow)*, 11:23, 1947.

[78] P. Ring and P. Schuck. *The nuclear many-body problem*. Springer-Verlag, 1980.

[79] J. Dobaczewski, H. Flocard, and J. Treiner. Hartree-fock-bogolyubov description of nuclei near the neutron-drip line. *Nuclear Physics A*, 422(1):103 – 139, 1984.

[80] P.G. de Gennes. *Superconductivity of Metals and Alloys*. Advances book classics. Addison-Wesley, 1989.

[81] H.T .C Stoof and M.Houbiers. Condensed matter physics with trapped atomic fermi. *Preprint cond-mat/9808171*, 1998.

[82] A. V. Avdeenkov and J. L. Bohn. Pair wave functions in atomic fermi condensates. *Phys. Rev. A*, 71:023609, Feb 2005.

[83] Generalized mean-field approach to a resonant bose-fermi mixture. *Physical Review A*, 78(6):063612, 2008.

[84] Stefano Giorgini, Lev P. Pitaevskii, and Sandro Stringari. Theory of ultracold atomic fermi gases. *Rev. Mod. Phys.*, 80:1215–1274, Oct 2008.

[85] D. C. E. Bortolotti, V. Avdeenkov Alexandr, Christopher Ticknor, and John L. Bohn. Bose-Fermi mixtures near an interspecies feshbach resonance: testing a non-equilibrium approach. *Journal of Physics B: Atomic, Molecular and Optical Physics*, 39:189, 2006.